

# Do the majority of stars form as gravitationally unbound?

František Dinnbier<sup>1</sup>, Pavel Kroupa<sup>1,2</sup> and Richard I. Anderson<sup>3</sup>

<sup>1</sup> Astronomical Institute, Faculty of Mathematics and Physics, Charles University, V Holešovičkách 2, 180 00 Praha 8, Czech Republic

e-mail: [dinnbier@sirrah.troja.mff.cuni.cz](mailto:dinnbier@sirrah.troja.mff.cuni.cz)

<sup>2</sup> Helmholtz-Institut für Strahlen- und Kernphysik, University of Bonn, Nussallee 14-16, 53115 Bonn, Germany

e-mail: [pavel@astro.uni-bonn.de](mailto:pavel@astro.uni-bonn.de)

<sup>3</sup> Institute of Physics, Laboratory of Astrophysics, École Polytechnique Fédérale de Lausanne (EPFL), Observatoire de Sauverny, 1290 Versoix, Switzerland

e-mail: [richard.anderson@epfl.ch](mailto:richard.anderson@epfl.ch)

Received January 19, 2022; accepted ??

## ABSTRACT

**Context.** Some of the youngest stars (age  $\leq 10$  Myr) are clustered, while many others are observed scattered throughout star forming regions or in complete isolation. It has been intensively debated whether the scattered or isolated stars originate in star clusters, or if they form truly isolated, which could help constrain the possibilities how massive stars are formed.

**Aims.** We adopt the assumption that all stars form in gravitationally bound star clusters embedded in molecular cloud cores ( $\Gamma$ -1 model), which expel their natal gas early after their formation, and compare the fraction of stars found in clusters with observational data.

**Methods.** The star clusters are modelled by the code NBODY6, which includes binary stars, stellar and circumbinary evolution, gas expulsion, and the external gravitational field of their host galaxy.

**Results.** We find that small changes in the assumptions in the current theoretical model estimating the fraction,  $\Gamma$ , of stars forming in embedded clusters have a large influence on the results, and we present a counterexample as an illustration. This calls into question theoretical arguments about  $\Gamma$  in embedded clusters, and it suggests that there is no firm theoretical ground for low  $\Gamma$  in galaxies with lower star formation rates (SFRs). Instead, the assumption that all stars form in embedded clusters is in agreement with observational data for the youngest stars (age  $\leq 10$  Myr). In the  $\Gamma$ -1 scenario, the observed fraction of the youngest stars in clusters increases with the SFR only weakly; the increase is caused by the presence of more massive clusters in galaxies with higher SFRs, which release fewer stars to the field in proportion to their mass. The  $\Gamma$ -1 model yields a higher fraction of stars in clusters for older stars (age between 10 Myr and 300 Myr) than what is observed. This discrepancy can be caused by initially less compact clusters and/or a slightly lower star formation efficiency than originally assumed in the  $\Gamma$ -1 model, or by interactions of the post gas expulsion revirialised open clusters with molecular clouds.

**Key words.** Galaxies: star formation, Galaxies: stellar content, Galaxies: star clusters: general

## 1. Introduction

Star formation takes place in the densest parts of molecular clouds. The youngest stars are usually found to be concentrated in embedded star clusters (Lada et al. 1991; Lada & Lada 2003; Megeath et al. 2016) or more dispersed throughout OB associations (Blaauw 1964). This opens two broad scenarios for the conditions for star formation.

In the first scenario, all stars form in gravitationally bound embedded clusters (e.g. Lada et al. 1984; Kroupa 1995b; Lada & Lada 2003; Porras et al. 2003; Kroupa et al. 2001; Banerjee & Kroupa 2017; González-Samaniego & Vazquez-Semadeni 2020), which form throughout a molecular cloud, which as a whole, might not be necessarily gravitationally bound, but merely a condensation in the interstellar medium. The clusters expand and lose a substantial fraction of their stars as the result of the expulsion of the non-star forming gas. Cores of some of these clusters survive the violent gas expulsion event (Lada et al. 1984; Boily & Kroupa 2003) and they are observed as gas-free open star

clusters, while the escaping stars are receding out of clusters, and they are observed as unbound OB associations. After gas expulsion, the surviving cluster still evaporates and ejects stars, albeit at a slower rate than during gas expulsion. Dynamical ejections are particularly important for the most massive stars in the cluster, where the process is able to kick tens of percent of OB stars from the cluster (Fujii & Portegies Zwart 2011; Oh et al. 2015; Oh & Kroupa 2016; Wang et al. 2019).

In the second scenario, stars form throughout the molecular cloud in hierarchical structures following the density field created by interstellar turbulence (e.g. Preibisch & Zinnecker 1999; Elmegreen 2000; Clark et al. 2005; Elmegreen et al. 2006). While some star formation occurs in initially bound clusters, a substantial amount of star formation occurs in initially non gravitationally bound groups. Thus, unlike in the first scenario, OB associations are gravitationally unbound from their formation.

In this context it is useful to define the fraction of star formation  $\Gamma = \text{CFR}/\text{SFR}$  occurring in initially gravitation-

ally bound embedded clusters. The CFR is the star formation rate within all bound clusters in the galaxy, and the SFR is the total star formation rate of the galaxy.

The two scenarios have deep implications not only for the formation of bound star clusters, but also for massive star formation, which still lacks a full understanding (Zinnecker & Yorke 2007). In the first scenario, massive stars are clustered, and they compete for the available gas with each other (Bonnell et al. 1997, 2001), lose their specific angular momentum in the process, which naturally leads to their primordial mass segregation. In clusters, more massive stars can be also produced by their mergers still in the pre-main-sequence stage (Bonnell et al. 1998). In contrast, the second scenario is based on forming massive stars in isolation, a process for which there is not much observational evidence (Selier et al. 2011).

In the Galaxy, observations suggest that the majority ( $\Gamma = 0.5$  to  $1.0$ ) of star formation occurs in embedded clusters (e.g. Carpenter et al. 1995; Carpenter 2000; Lada & Lada 2003; Porras et al. 2003; Bressert et al. 2010; Winston et al. 2020). An independent piece of evidence for  $\Gamma$  close to 1 comes from the observed lower binary fraction of field stars in contrast to the binary fraction in star forming regions, which can be explained as a result of dynamical processing within clusters (Kroupa 1995a,b; Marks & Kroupa 2011). When focusing on O stars, only 20 % to 50% of them are located in the field (i.e. outside clusters or OB associations) (Mason et al. 1998), but many of the field O stars are unambiguously identified as runaway stars originating from bound systems (e.g. Blaauw 1964; Stone 1991; Tetzlaff et al. 2011; Gvaramadze et al. 2012), further decreasing the upper limit of the truly isolated massive star formation.

In contrast, some observations of external galaxies point to a substantially lower values of  $\Gamma$  of the order of 0.1 (e.g. Goddard et al. 2010; Adamo et al. 2011; Johnson et al. 2016). Kruijssen (2012) suggests a semi-analytic model, according to which  $\Gamma$  increases with the star formation rate of the galaxy per unit area  $\Sigma_{\text{SFR}}$ . However, later Chandar et al. (2017) found substantially larger values of  $\Gamma$  in galaxies with low  $\Sigma_{\text{SFR}}$ , and also no clear dependence of  $\Gamma$  on the  $\Sigma_{\text{SFR}}$ . They suggest that the dependency previously reported was caused by an age biased sample. Likewise, Fensch et al. (2019) report large values of  $\Gamma$  in tidal dwarf galaxies located around galaxy NGC 5291, which differ by  $\approx 3\sigma$  from the estimate by Kruijssen (2012). Stephens et al. (2017) select a sample of well-isolated massive young stellar objects in the Large Magellanic Cloud (LMC), previously thought to be massive stars formed in isolation, and find that each of them is surrounded by a star cluster of  $\geq 100$  stars, indicating that the vast majority ( $\geq 95$  %) of massive stars form in clusters instead of in isolation. Thus, it is possible that the vast majority (if not all) massive stars found currently in isolation in external galaxies, are in reality runaway stars, or they are surrounded by a small star cluster consisting of lower mass stars, which is not resolvable within the given survey.

In the present paper, we assume that all stars form in gravitationally bound embedded clusters ( $\Gamma = 1$ ), which evolve due to their cluster dynamics, gas expulsion, stellar evolution from a realistic initial stellar mass function (IMF), and the tidal field of their host galaxy. We study the fraction of stars to be found within the clusters as a function of the cluster age, mass, orbital radius within the galaxy,

and we synthesize these results for a population of star clusters for a galaxy of a given global star formation rate in the framework of the integrated galactic initial mass function (IGIMF), and provide a comparison to observational data. Our assumption of  $\Gamma = 1$  contrasts with the theoretical value of  $\approx 0.1$  as expected for a Milky Way-like galaxy from the theoretical model of Kruijssen (2012), which provides  $\Gamma$  as a function of the properties of the galaxy, and which favours isolated massive star formation in galaxies with lower star formation rates. We question some of the assumptions used in the theoretical model, and we illustrate on a simple example its main limitations.

## 2. The current model for $\Gamma$ and its limitations

### 2.1. Overview of the model

Kruijssen (2012) (hereafter K12) presented the first (and the only known to us) theoretical framework to infer  $\Gamma$  from the properties of the interstellar medium (ISM) of the particular galaxy. The model assumes that the probability density function  $dp/dx$  of the ISM mass density is log-normal, and that star formation proceeds at a constant rate per free-fall time, so the denser gas produces stars more rapidly. The variable  $x$  denotes the normalised local density contrast,  $x = \rho/\rho_{\text{ISM}}$ , where  $\rho_{\text{ISM}}$  is the midplane density. Star formation is terminated either by gas exhaustion, by supernova feedback, or it still continues up to the age of interest. If star formation terminates by gas exhaustion, the final star formation efficiency (SFE  $\equiv$  stellar mass/(stellar plus gaseous mass)) is set to 0.5, which is motivated by the reduction of the stellar mass by protostellar outflows. If star formation is terminated by feedback from newly formed stars, the termination time is calculated by balancing the thermal pressure due to feedback with the turbulent pressure of the ISM.

The fraction of stars  $\gamma$ , which form in gravitationally bound clusters is estimated to be linearly proportional to the SFE, i.e.  $\gamma = 2 \text{SFE}$  (the factor 2 is to reach  $\gamma = 1$  for the maximum allowed SFE of 0.5). The clusters are subjected to tidal fields of passing interstellar clouds, which dissolve all clusters, which formed at normalised density below  $x_{\text{cce}}$  on a time-scale shorter than the specified age limit, which is chosen to be 10 Myr; clusters formed in gas above this density are assumed to be intact. Then, the fraction of stars which form in gravitationally bound clusters is calculated as

$$\Gamma = \frac{\int_{x_{\text{cce}}}^{\infty} \gamma(x) \text{SFE}(x) x (dp/dx) dx}{\int_{-\infty}^{\infty} \text{SFE}(x) x (dp/dx) dx}. \quad (1)$$

Since all the dependent variables under the integral sign as well as  $x_{\text{cce}}$  depend implicitly on the galactic parameters  $\Sigma_{\text{g}}$  (mean gas surface density),  $\Omega$  (angular frequency) and  $Q$  (Toomre parameter),  $\Gamma$  can be expressed as a function of these three galactic parameters. Further simplification is obtained by expressing the star formation rate  $\Sigma_{\text{SFR}}$  of the galaxy by  $\Sigma_{\text{g}}$  according to the Schmidt star formation law (Schmidt 1959; Kennicutt 1998). Taking typical values for the two other parameters ( $\Omega$  and  $Q$ ), K12 arrived at a formula for  $\Gamma$  as a function of  $\Sigma_{\text{SFR}}$  only. Because of this property, we refer to this model as the  $\Gamma$ - $\Sigma_{\text{SFR}}$  model hereafter in this work.

## 2.2. Limitations of the model

The  $\Gamma$ - $\Sigma_{\text{SFR}}$  model provides a valuable theoretical formulation for understanding the functional dependence of physical quantities. However, its derivation requires several simplifications or assumptions that require further consideration because they significantly affect model predictions. In particular:

- Probably the most significant simplification is the absence of the threshold for star formation of  $\approx 120 M_{\odot} \text{ pc}^{-2}$  (Lada et al. 2009, 2010; Heiderman et al. 2010), which suggests that star formation in the Galaxy is absent at gas densities below  $n(\text{H}_2) \approx 10^4 \text{ cm}^{-3}$  ( $\approx 300 M_{\odot} \text{ pc}^{-3}$ ). For the normalised density contrast, this means that star formation occurs only at  $x_{\text{lim}} \gtrsim 10^4$  (for a Milky Way-like galaxy), while the  $\Gamma$ - $\Sigma_{\text{SFR}}$  model provides a much lower threshold of  $x_{\text{cce}} \approx 10^2$  for bound cluster formation and survival (Sect. 2.7.3 in K12). The model even considers scattered star formation at gas densities below  $x = 10^2$  (cf. their figure 1), i.e. at densities  $n(\text{H}_2) \lesssim 10^2 \text{ cm}^{-3}$ . The low star formation threshold results in many stars forming as gravitationally unbound, leading to low values of  $\Gamma$ .
- The  $\Gamma$ - $\Sigma_{\text{SFR}}$  model assumes (Sect. 2.5.2 in K12) that star formation proceeds at a constant rate until it is quenched by supernovae (which occur at earliest at 3 Myr after massive star formation started), or alternatively by radiation pressure. This neglects the influence of important early forms of stellar feedback, e.g. the photoionising radiation and stellar winds, which have a strong impact on the surrounding gas, substantially dispersing the natal cloud before the first supernova occurs (e.g. Rogers & Pittard 2013; Gavagnin et al. 2017; Haid et al. 2018; Dinnbier & Walch 2020). Neglecting early stellar feedback likely overestimates the value of  $\text{SFE}(x)$ .
- The functional form of the probability density function of self-gravitating star forming gas, which is a power-law function of a slope close to  $-2$  (e.g. Kritsuk et al. 2011; Schneider et al. 2013; Lombardi et al. 2015; Chen et al. 2018) is very different from the log-normal distribution of non-self-gravitating turbulent ISM (Vazquez-Semadeni 1994; Padoan et al. 1997; Kritsuk et al. 2011) as assumed in the  $\Gamma$ - $\Sigma_{\text{SFR}}$  model.
- As the collapse of the star forming cloud proceeds, its free-fall time-scale decreases because density increases. Conversely, the  $\Gamma$ - $\Sigma_{\text{SFR}}$  model assumes a constant SFR with time (Eq. 22 in K12).
- To derive the density threshold  $x_{\text{cce}}$  (Sect. 2.7 in K12), it is assumed that the ISM velocity dispersion  $\sigma_{\text{g}}$  is constant regardless of the distance between the clumps. This is a reasonable approximation for the relative velocity between two molecular clouds. However, for the scale-free ISM within a given cloud,  $\sigma_{\text{g}}$  depends on distance  $l$  between the target cluster and the clump according to the Larson relations (e.g. Larson 1981; Heyer et al. 2009).
- The  $\Gamma$ - $\Sigma_{\text{SFR}}$  model assumes that all molecular clouds are of the same mass (eq. 35 in K12).
- The  $\Gamma$ - $\Sigma_{\text{SFR}}$  model does not consider star cluster dynamics, which can eject a substantial fraction of young massive stars from clusters even during the first several Myr of the cluster's existence (Perets & Šubr 2012; Oh et al. 2015; Wang et al. 2019), thus underestimating  $\Gamma$ .

- Expulsion of the non-star forming gas is not considered. Instead, it is assumed that most of the gas is consumed by star formation, which is not reproduced by many of the more recent star forming simulations (e.g. Colín et al. 2013; Gavagnin et al. 2017; González-Samaniego & Vazquez-Semadeni 2020).

In order to illustrate the strong dependence of the  $\Gamma$ - $\Sigma_{\text{SFR}}$  model on its assumptions, we consider a very simple model for star formation that agrees with most observational facts, yet leads to completely different results than the  $\Gamma$ - $\Sigma_{\text{SFR}}$  model. We stress that we use this as an illustration only and do not claim that star formation occurs according to this toy model. Rather, we argue that a radically different approach is needed to tackle the highly non-linear process of clustered star formation from a theoretical perspective. Consider that all stars form only at density  $x > x_{\text{lim}}$ , and star formation occurs in gravitationally bound clusters if  $x > x_{\text{cce}}$ , and in unbound associations if  $x < x_{\text{cce}}$ . It means that  $\gamma(x) = 1$  for  $x > x_{\text{cce}}$  and 0 otherwise. We further assume that  $\text{SFE}(x) = 1/3$  regardless of  $x$  (e.g. Geyer & Burkert 2001; Kroupa et al. 2001; Megeath et al. 2016; Banerjee & Kroupa 2017; Geen et al. 2018). From eq. (1), these assumptions lead to  $\Gamma = 1$  for galaxies with  $x_{\text{cce}} < x_{\text{lim}}$ , and  $\Gamma$  decreasing with  $x_{\text{cce}}$  for  $x_{\text{cce}} > x_{\text{lim}}$ , with  $x_{\text{cce}} = x_{\text{lim}}$  at  $\log_{10}(\rho_{\text{ISM}}[\text{g cm}^{-3}]) \approx -21.8$  (taking aside the weaker dependence on  $\Omega$  and  $Q$ , we note that  $x_{\text{cce}}$  can be used as a proxy for  $\Sigma_{\text{SFR}}$ ). This model is in a stark contrast to the  $\Gamma$ - $\Sigma_{\text{SFR}}$  model, where  $\Gamma \approx 0.1$  for galaxies with low  $x_{\text{cce}}$  of  $\approx 10^2$ , which increases with  $x_{\text{cce}}$  towards  $\approx 0.7$ .

By choosing different functional forms for  $\gamma(x)$  and  $\text{SFE}(x)$ , neither of which are well constrained, it is easy to find an almost arbitrary dependence of  $\Gamma$  on  $x_{\text{cce}}$ , and therefore on  $\Sigma_{\text{SFR}}$ . The extreme sensitivity on initial assumptions<sup>1</sup> is caused by recursively substituting equations into another, several of which are non-linear or contain terms of uncertain importance.

This behaviour is typical for chaotic systems, which cannot be understood by linearising or simplifying relevant equations. Thus, redoing the analysis for the  $\Gamma$ - $\Sigma_{\text{SFR}}$  model in the same way will not yield more reliable results even if the aforementioned issues are resolved.

The above toy model illustrates that even minor changes in the assumptions of the  $\Gamma$ - $\Sigma_{\text{SFR}}$  model lead to drastically different outcomes and thus questions the previously suggested theoretical result that most stars form in gravitationally unbound entities in a Milky Way-like galaxy.

In the following, we have therefore adopted the opposite approach, namely that all stars form in gravitationally bound embedded clusters (i.e.  $\Gamma = 1$ ), to investigate the currently observed fraction of bound stars by dynamical N-body simulations. The assumption of  $\Gamma = 1$  is motivated by observational surveys of pre-main sequence stars in molecular clouds (e.g. Lada et al. 1991; Megeath et al. 2016; Joncour et al. 2018), the distribution functions of binary stars in the Galactic field in comparison to star forming regions (e.g. Reipurth & Zinnecker 1993; Leinert et al. 1993; Kroupa 1995a), and the general argument that a star forming molecular cloud core is observed to always contain

<sup>1</sup> The sensitivity to the choice of the particular functional forms was mentioned by Kruijssen (2012, their appendix D), although its influence on results was not investigated or discussed in detail.

significantly more gas than the weight of a single late-type star (Alves et al. 2007; Goodwin et al. 2008). We refer to the present model as  $\Gamma$ -1 model to distinguish it from the  $\Gamma$ - $\Sigma_{\text{SFR}}$  model.

Further assumptions of the  $\Gamma$ -1 model are that the clusters are initially compact (half-mass radii  $r_h$  of  $\lesssim 1$  pc for clusters of mass  $M_{\text{ecl}} \lesssim 10^4 M_\odot$ ). The initial cluster mass function is a power-law (eq. 4), whose slope and upper mass limit follows from the galactic star forming rate as obtained from the IGIMF theory (Kroupa & Weidner 2003). The clusters form with SFE = 1/3, and they expel their non-star forming gas on the timescale of  $r_h/10 \text{ km s}^{-1} \approx 0.05 \text{ Myr}$  at the cluster age of 0.6 Myr.

The particular values of the parameters in the  $\Gamma$ -1 model might be adjusted in the future when more accurate observational data become available. This iteration could provide another constraint on the birth properties of star clusters.

### 3. Model description and numerical method

#### 3.1. Model description

The main results of this article are based on the models presented in Sect. 3.1.1 and correspond to the most probable initial conditions for embedded star clusters (standard models). To assess the dependence on the particular choice of initial assumptions, we compute additional models to investigate the influence of the initial cluster radius, the SFE, and primordial mass segregation (Sect. 3.1.2).

##### 3.1.1. Standard models

Observed open clusters are well described by the Plummer model (e.g. Röser et al. 2011; Röser & Schilbach 2019) and star forming molecular cloud filaments have Plummer-like cross sections (e.g. André et al. 2014), which motivates us to use this description as initial conditions for present models. The Plummer model is described by its stellar mass,  $M_{\text{ecl}}$ , and Plummer parameter,  $a_{\text{ecl}}$ . The Plummer parameter is related to the cluster mass by the mass-radius relation of Marks & Kroupa (2012), where

$$\frac{a_{\text{ecl}}}{\text{pc}} = 0.077 \left( \frac{M_{\text{ecl}}}{M_\odot} \right)^{1/8}. \quad (2)$$

The stellar masses of the clusters in our model grid are  $50 M_\odot$ ,  $100 M_\odot$ ,  $\dots$   $6400 M_\odot$ , which approximately covers the mass range of observed star clusters in the Galaxy and the galaxy M 31. To obtain better statistics, we simulate the  $50 M_\odot$  clusters 256 times with different random seed,  $100 M_\odot$  clusters 128 times etc., so the  $6400 M_\odot$  clusters are simulated twice.

Stellar masses are sampled from the Kroupa (2001) model of the initial mass function (IMF) in the mass range ( $0.08 M_\odot, m_{\text{max}}$ ). To allow only the more massive clusters to form massive stars, we adopt the  $m_{\text{max}} - M_{\text{ecl}}$  relation from Weidner et al. (2010) (see also Elmegreen 1983, 2000 for earlier works on the same topic). Initial conditions for the clusters are generated by the software package MCLUSTER, which is described in Küpper et al. (2011). Initially, all stars are in binaries. Stars with mass below  $3 M_\odot$  have the distribution of orbital periods according to Kroupa (1995a), while stars more massive than that have the distribution of

orbital periods of Sana et al. (2012), which generally results in more compact systems.

The expulsion of the gas which was not consumed by the forming stars has a profound impact on cluster dynamics (e.g. Tutukov 1978; Lada et al. 1984; Goodwin 1997; Kroupa et al. 2001; Geyer & Burkert 2001; Banerjee & Kroupa 2013, 2017). We approximate the gaseous component by a Plummer potential with  $a_{\text{ecl}}$  identical to that of the stellar component, and of mass  $2M_{\text{ecl}}$ , so we assume the SFE to be 33 %. When the embedded phase ends at time  $t_d = 0.6 \text{ Myr}$ , the mass of the gaseous component is reduced exponentially on the time scale  $\tau_M = 1.3a_{\text{ecl}}/10 \text{ km s}^{-1} \approx 0.04 \text{ Myr}$ ; it is the same approximation as used by Kroupa et al. (2001).

To study stellar escape from star clusters realistically, one needs to include the tidal forces due to the host galaxy. Accordingly, we adopt the galactic potential of Allen & Santillan (1991), which consists of the disc, halo and the central part of the galaxy. The modelled clusters orbit the galaxy on circular trajectories of radii  $R_g = 4 \text{ kpc}$ ,  $R_g = 8 \text{ kpc}$  and  $R_g = 12 \text{ kpc}$ . All these models are calculated for stars of Solar metallicity ( $Z = 0.014$ ). In addition, we calculate clusters with the subsolar metallicities of  $Z = 0.006$  and  $Z = 0.002$  orbiting at  $R_g = 8 \text{ kpc}$ .

##### 3.1.2. Models for exploring the sensitivity on initial conditions

We study the influence of the particular functional form between the Plummer parameter and cluster mass, i.e.  $a_{\text{ecl}} = a_{\text{ecl}}(M_{\text{ecl}})$ . In these models, we assume that

$$\frac{a_{\text{ecl}}}{\text{pc}} = 0.034 \left( \frac{M_{\text{ecl}}}{M_\odot} \right)^{1/3}, \quad (3)$$

which presents a stronger mass dependence than in the standard models (eq. 2). Normalisation of eq. (3) is chosen so that the least massive clusters ( $M_{\text{ecl}} = 50 M_\odot$ ) have the same half-mass radius ( $r_h = 0.163 \text{ pc}$ ) as clusters of the same mass in standard models. The most massive clusters in our models ( $M_{\text{ecl}} = 6400 M_\odot$ ) have a half-mass radius of  $0.79 \text{ pc}$  according to eq. (3), while it is  $0.30 \text{ pc}$  in standard models. The form of eq. (3) means that embedded clusters have the same density regardless of their mass. In discussion, we refer to these models as "A" models, while standard models are referred to "S" models.

Another quantity of interest is the SFE, which we decrease to 0.25. Otherwise, the clusters are identical as in the standard models. In discussion, we refer to these models as "F" models. "A" and "F" models are calculated for the same library of clusters as the standard models with  $R_g = 8 \text{ kpc}$  and  $Z = 0.014$ , but we realised all clusters of mass  $\leq 400 M_\odot$  only 32 times.

We also study the influence of primordial mass segregation (Sect. 5.1). These models are generated according to the recipe of Šubr et al. (2008) with mass segregation index  $S = 0.5$ . This results in highly mass segregated clusters; for example, the half-mass radius of M stars is  $0.4 \text{ pc}$ , while the half-mass radius of B stars is  $0.1 \text{ pc}$ . Otherwise, the models are identical to the standard models. The role of primordial mass segregation is studied only in  $M_{\text{ecl}} = 400 M_\odot$  clusters orbiting at  $R_g = 8 \text{ kpc}$  and with  $Z = 0.014$ . Similar to the standard models, we simulate each  $400 M_\odot$  cluster 32 times with different random seeds. These models are labelled "M" models.

### 3.2. Numerical method

The clusters are integrated by the code NBODY6, which uses a 4th order Hermite predictor-corrector (Makino 1991), quantised time-steps with the Ahmad-Cohen method (Ahmad & Cohen 1973; Makino & Aarseth 1992). Compact subsystems of two, three and more stars are handled by regularising techniques (Kustaanheimo & Stiefel 1965; Aarseth & Zare 1974; Mikkola & Aarseth 1990). Metallicity-dependent stellar evolution is included (Tout et al. 1996; Hurley et al. 2000) as well as an approximation to circumbinary evolution including Roche mass transfer and common-envelope evolution (Hurley et al. 2002). A detailed description of the algorithms used in NBODY6 is provided in Aarseth (2003).

## 4. Results

For the purpose of this work, we define a star cluster as a group of at least 10 centre of mass bodies which are gravitationally bound. The fraction  $f_{\text{IC}}$  of stars in clusters is the number of stars in clusters  $N_{\text{in}}$  divided by the sum of stars in clusters  $N_{\text{in}}$  and in the field  $N_{\text{out}}$ . We discuss  $f_{\text{IC}}$  in different contexts:  $f_{\text{IC}}(M_{\text{ecl}})$ ,  $f_{\text{IC, pop}}$  and  $f_{\text{IC}}(m)$  is the fraction of stars in clusters for clusters of mass  $M_{\text{ecl}}$ , for the whole population of star clusters which formed according to a given initial cluster mass function, and for stars of stellar mass  $m$  formed by a whole population of star clusters, respectively. The time averaged fraction of stars in age interval  $\Delta t$  formed by the whole cluster population is denoted  $\bar{f}_{\text{IC, pop}}(\Delta t)$ , and the likely observed fraction of these stars in clusters is denoted  $\bar{f}_{\text{IC, pop}}^{\text{obs}}(\Delta t)$ .

We assume two idealised scenarios for the star formation history. In the first one, all star clusters are formed in a single starburst of a short ( $\lesssim 10$  Myr) duration with no star formation afterwards (Sect. 4.2 and 4.3). In the second one, star formation proceeds continuously with a constant star formation rate (SFR; Sect. 4.4). A comparison with observational data and discussion of the most likely value of  $\Gamma$  is discussed in Sect. 4.5.

### 4.1. The dependence on cluster mass

The fraction  $f_{\text{IC}}(M_{\text{ecl}})$  of stars in clusters for clusters of different mass,  $M_{\text{ecl}}$ , as a function of cluster age,  $t$ , is shown in Fig. 1. These clusters orbit the galaxy at the radius  $R_{\text{g}} = 8$  kpc, and have a metallicity  $Z = 0.014$ . This plot includes stars of all spectral types. The rapid decrease of  $f_{\text{IC}}(M_{\text{ecl}})$  during the first  $\approx 15$  Myr is caused by the reaction of the cluster to gas expulsion. After that, the decrease of  $f_{\text{IC}}(M_{\text{ecl}})$  slows down, where more massive clusters retain more stars at a given time. By 300 Myr, all the clusters with initial mass  $M_{\text{ecl}} \lesssim 400 M_{\odot}$  released more than 95% of their stars to the field, while clusters with  $M_{\text{ecl}} = 6400 M_{\odot}$  released only 40% of their stars into the field. An estimate of the fraction of stars in clusters, which is likely to be observed, is shown in the left panel of Fig. A.1.

The decrease of  $f_{\text{IC}}(M_{\text{ecl}})$  with decreasing  $M_{\text{ecl}}$  is expected as lower mass clusters are impacted more by gas expulsion (Baumgardt & Kroupa 2007), and have a shorter median two-body relaxation time-scale which leads to more rapid evaporation and cluster dissolution (Baumgardt & Makino 2003; Lamers et al. 2005).

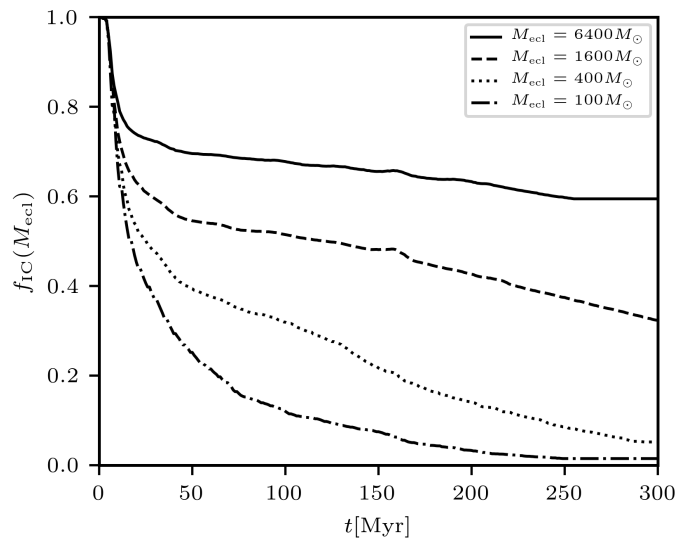


**Fig. 1.** The fraction of all stars which are present in their birth clusters at a given age  $t$  for clusters of initial mass  $M_{\text{ecl}} = 100 M_{\odot}$  (dash-dotted line),  $M_{\text{ecl}} = 400 M_{\odot}$  (dotted line),  $M_{\text{ecl}} = 1600 M_{\odot}$  (dashed line), and  $M_{\text{ecl}} = 6400 M_{\odot}$  (solid line).

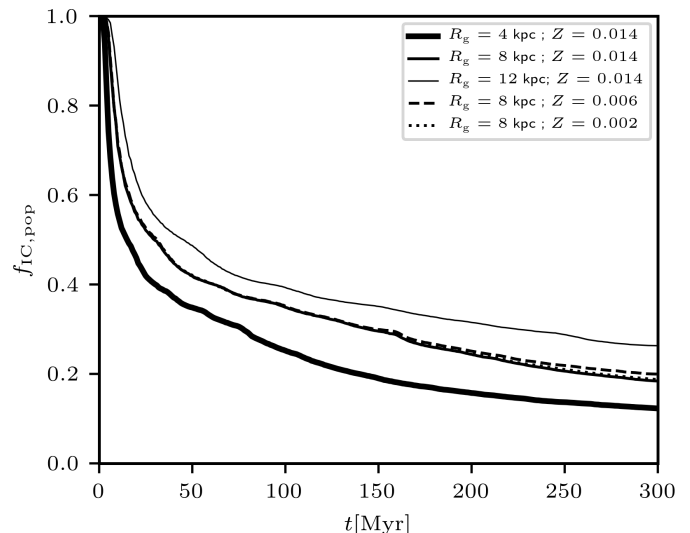


**Fig. 2.** The fraction of all stars located in their parent cluster for the galaxy-wide ECMF of eq. (4) and for a single star-burst. Clusters orbit the galaxy at  $R_{\text{g}} = 4$  kpc,  $R_{\text{g}} = 8$  kpc, and  $R_{\text{g}} = 12$  kpc (different thickness of solid lines). These clusters have the Solar metallicity of  $Z = 0.014$ . Models of  $Z = 0.006$  and  $Z = 0.002$  for  $R_{\text{g}} = 8$  kpc are shown by the dashed and dotted lines.

### 4.2. The galaxy wide fraction of stars in clusters in a single starburst

We assume that embedded clusters are distributed according to the embedded cluster mass function (ECMF),

$$\xi_{\text{ecl}}(M_{\text{ecl}}) \equiv \frac{dN_{\text{ecl}}}{dM_{\text{ecl}}} \propto M_{\text{ecl}}^{-\beta}, \quad (4)$$

where  $dN_{\text{ecl}}$  is the number of clusters in the mass bin  $(M_{\text{ecl}}, M_{\text{ecl}} + dM_{\text{ecl}})$ , and the index  $\beta$  is a parameter obtained from observations. Let a cluster of mass  $M_{\text{ecl}}$  have a property  $q(M_{\text{ecl}})$ , which is normalised by the total number of stars ( $q$  can be for example  $f_{\text{IC}}$ ). Then, for a coeval popu-

lation of star clusters with mass range  $(M_{\text{ecl,min}}, M_{\text{ecl,max}})$ ,

$$q_{\text{pop}} = \frac{\int_{M_{\text{ecl,min}}}^{M_{\text{ecl,max}}} \xi_{\text{ecl}}(M_{\text{ecl}}) q(M_{\text{ecl}}) M_{\text{ecl}} dM_{\text{ecl}}}{\int_{M_{\text{ecl,min}}}^{M_{\text{ecl,max}}} \xi_{\text{ecl}}(M_{\text{ecl}}) M_{\text{ecl}} dM_{\text{ecl}}}. \quad (5)$$

We note that the integrals are mass weighted because the contribution of each mass bin  $dM_{\text{ecl}}$  is proportional to the total number of stars which formed within the mass bin, and thus in turn to the cluster mass  $M_{\text{ecl}}$ . In the following text, we refer to a quantity calculated by eq. (5) as galaxy-wide. In the Galaxy and nearby galaxies,  $\beta \approx 2$  (van den Bergh & Lafontaine 1984; Whitmore et al. 1999; Larsen 2002; Lada & Lada 2003; Bik et al. 2003; de la Fuente Marcos & de la Fuente Marcos 2004; Gieles et al. 2006), and the cluster mass range covers approximately an interval of  $(30 M_{\odot}, 10^4 M_{\odot})$  (Johnson et al. 2017).

For an ECMF with these parameters, we obtain the time dependence of the galaxy wide fraction  $f_{\text{IC,pop}}$  of stars in clusters as shown in Fig. 2. We assume that all the clusters were formed in a single starburst, i.e. that they are coeval. The plot is constructed for clusters orbiting at different galactocentric radii  $R_g$ , and with different metallicities for  $R_g = 8$  kpc. For all models,  $f_{\text{IC,pop}}$  drops significantly during the first 50 Myr of cluster evolution. This drop is dominated by the early gas expulsion, with the galactic tidal field being of secondary importance. At a given time, the value of  $f_{\text{IC,pop}}$  increases with increasing  $R_g$  as the tidal field of the galaxy becomes less important. In particular, at 200 Myr and for  $R_g = 4$  kpc, 8 kpc and 12 kpc,  $f_{\text{IC,pop}} = 0.16, 0.25$  and 0.32, respectively.

The models with subsolar metallicities of  $Z = 0.002$  and  $Z = 0.006$  are shown by the dotted and dashed lines in Fig. 2, respectively. They indicate that  $f_{\text{IC,pop}}$  is practically independent of the metallicity of the clusters.

Fig. 3 shows the time dependence of the galaxy-wide fraction  $f_{\text{IC,pop}}(m)$  of stars in clusters for stars of different masses  $m$  (or equivalently different spectral types). The figure demonstrates that the clusters mass segregate because the probability to find more massive stars (with the exception of O stars) in clusters at a given time is larger than to find there lower mass stars. The mass segregation is dynamical because these models are free of primordial mass segregation. At a given time, the fraction  $f_{\text{IC,pop}}(m)$  monotonically increases with stellar mass apart from the O stars, because many O stars are ejected in close three- and many- body interactions producing runaway stars (e.g. Fujii & Portegies Zwart 2011; Tanikawa et al. 2012; Perets & Šubr 2012; Oh & Kroupa 2016). At the age of 200 Myr, only 19% of M stars are located in clusters, while 32% of late B stars are located in clusters.

#### 4.3. Fraction of stars in clusters in the context of the IGIMF in a single starburst

We explore the behaviour of  $f_{\text{IC,pop}}$  in the IGIMF framework, which was proposed by Kroupa & Weidner (2003) and further developed and refined by Weidner et al. (2013); Yan et al. (2017) and Jeřábková et al. (2018). According to the IGIMF theory, the upper mass limit for star clusters  $M_{\text{ecl,max}}$  increases, and  $\beta$  decreases with increasing the SFR, so environments with larger SFR tend to form more massive clusters, and these clusters are more abundant relative to the lower mass clusters. The SFR is taken from the

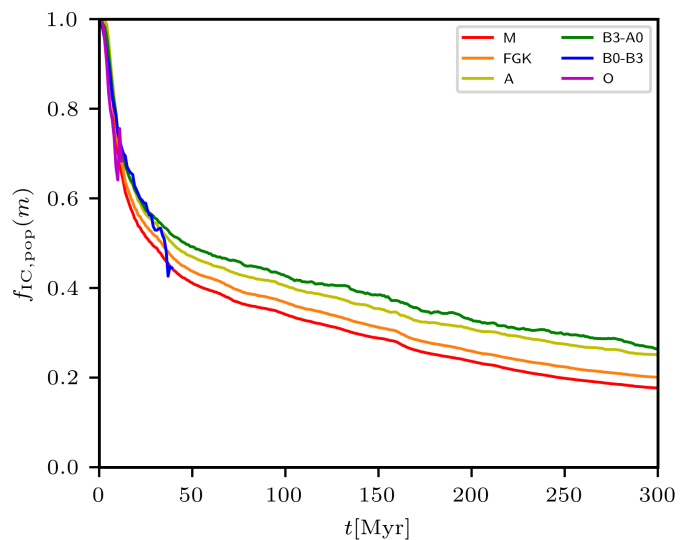


**Fig. 3.** The time dependence of the fraction of M (red line), F-K (orange), A (yellow), late B (green), early B (blue) and O (magenta) stars located in clusters for clusters with  $R_g = 8$  kpc and  $Z = 0.014$ . The clusters are assumed to form with the ECMF of eq. (4) with  $\beta = 2$ ,  $M_{\text{ecl,min}} = 30 M_{\odot}$ , and  $M_{\text{ecl,max}} = 10^4 M_{\odot}$ . At a given time,  $f_{\text{IC,pop}}(m)$  increases with stellar mass (apart from O stars), which is a result of dynamically induced mass segregation. O stars are slightly depleted in clusters because of their dynamical ejections.

whole galaxy. Thus, the IGIMF theory allows the calculation of a galaxy-wide stellar population assuming all stars form in embedded star clusters. It successfully couples the molecular cloud-core scale to galaxy-wide properties such as the star formation rate.

We study galaxies with SFRs of  $0.01 M_{\odot} \text{ yr}^{-1}$ ,  $0.1 M_{\odot} \text{ yr}^{-1}$ ,  $1 M_{\odot} \text{ yr}^{-1}$ ,  $10 M_{\odot} \text{ yr}^{-1}$  and  $100 M_{\odot} \text{ yr}^{-1}$ . For each of these galaxies, we determine the mass of the most massive cluster according to eq. 6 of Weidner et al. (2004) (see also Randriamanakoto et al. 2013), which reads

$$M_{\text{ecl,max}} = 8.5 \times 10^4 M_{\odot} (\text{SFR} / (M_{\odot} \text{ yr}^{-1}))^{0.75}. \quad (6)$$

Since galaxies with  $\text{SFR} \gtrsim 0.1 M_{\odot} \text{ yr}^{-1}$  form clusters more massive than we can simulate easily (a  $100 M_{\odot} \text{ yr}^{-1}$  galaxy has  $M_{\text{ecl,max}} = 2.7 \times 10^6 M_{\odot}$  according to eq. (6), which is beyond the capability of even the most dedicated current software; Wang et al. 2015, 2020), we extrapolate<sup>2</sup>  $f_{\text{IC}}(M_{\text{ecl}})$  from the five most massive clusters in our simulations towards higher mass at any time  $t$ . The least massive clusters dissolve early, so we did not calculate extra models for  $M_{\text{ecl}} < 50 M_{\odot}$ , but extrapolate the values of  $f_{\text{IC}}(M_{\text{ecl}})$  from the five least massive clusters in our simulations towards lower cluster mass.

The galaxy-wide fraction of stars in clusters as calculated by eq. (5) is shown in Fig. 4. We assume that all the

<sup>2</sup> From the requirement that the extrapolation function tends to 1 for  $M_{\text{ecl}} \rightarrow \infty$  and to 0 for  $M_{\text{ecl}} \rightarrow 0$ , we adopt the extrapolation function in the form of

$$y(\log_{10}(M_{\text{ecl}})) = \frac{1}{\pi} \left\{ \frac{\pi}{2} + \arctan(a(\log_{10}(M_{\text{ecl}})) - b) \right\}, \quad (7)$$

where  $a$  and  $b$  are the unknowns.

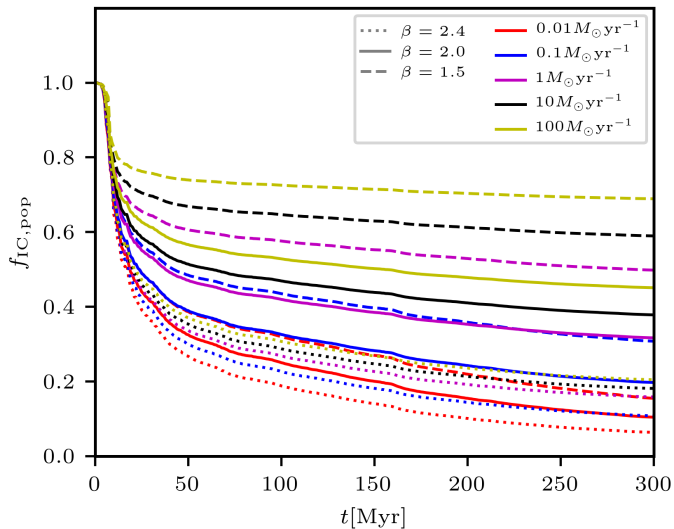


**Fig. 4.** The time dependence of the galaxy-wide  $f_{\text{IC,pop}}$  for galaxies with SFRs of  $0.01 M_{\odot} \text{ yr}^{-1}$ ,  $0.1 M_{\odot} \text{ yr}^{-1}$ ,  $1 M_{\odot} \text{ yr}^{-1}$ ,  $10 M_{\odot} \text{ yr}^{-1}$  and  $100 M_{\odot} \text{ yr}^{-1}$  (indicated by line colour) according to the IGIMF theory. The clusters have a metallicity of  $Z = 0.014$  and orbit the galaxy at  $R_g = 8 \text{ kpc}$ . The cluster mass range spans from  $5 M_{\odot}$  to  $M_{\text{ecl,max}}(\text{SFR})$ , which is given by eq. (6). For each value of the SFR, we consider  $\beta = 1.5$  (dashed lines),  $\beta = 2$  (solid lines), and  $\beta = 2.4$  (dotted lines).

clusters were formed at the same time. In order to be consistent with the IGIMF framework, we set the ranges of the ECMF to be  $M_{\text{ecl,min}} = 5 M_{\odot}$  and  $M_{\text{ecl,max}}$  according to eq. (6), which is different from the cluster population studied in Sect. 4.2. Here, we take  $\beta$  and the SFR as independent variables to explore the admitted uncertainty in  $f_{\text{IC,pop}}$ ; although in the strict sense of the IGIMF theory,  $\beta$  is a function of the SFR. According to the IGIMF theory,  $\beta$  ranges from 2.2 to 1.8 (Weidner et al. 2004; Jeřábková et al. 2018) in the considered range of the SFR of  $\text{SFR} = 0.01 M_{\odot} \text{ yr}^{-1}$  to  $\text{SFR} = 100 M_{\odot} \text{ yr}^{-1}$ . This is well within the extreme values of  $\beta$  of 1.5 and 2.4 considered in this work.

For any  $\beta$ , at a given time,  $f_{\text{IC,pop}}$  increases with increasing SFR because of the increase of  $M_{\text{ecl,max}}$ . Particularly, for  $\beta = 2$  at  $t = 200 \text{ Myr}$ ,  $f_{\text{IC,pop}} = 0.15$ ,  $0.35$  and  $0.48$  for SFR of  $0.01 M_{\odot} \text{ yr}^{-1}$ ,  $1 M_{\odot} \text{ yr}^{-1}$  and  $100 M_{\odot} \text{ yr}^{-1}$ , respectively. The ECMF of a shallower slope of  $\beta = 1.5$  (dashed lines in Fig. 4) produces more massive clusters relative to the lower mass ones, these clusters dissolve at a slower rate, which results in an increase of  $f_{\text{IC,pop}}$  at a given time. In contrast, ECMFs of a steeper slope ( $\beta = 2.4$ ; dotted lines) form more low mass clusters, which are easily disrupted, which results in a lower value of  $f_{\text{IC,pop}}$ . The likely observed fraction of stars in clusters within a galaxy of  $\text{SFR} = 1 M_{\odot} \text{ yr}^{-1}$  (Milky Way-like SFR) in the IGIMF theory (but with  $\beta$  taken as a free parameter) is shown in the right panel of Fig. A.1.

#### 4.4. Fraction of stars in clusters for a galaxy with a constant rate of star formation

In the previous two sections, Sect. 4.2 and 4.3, we studied  $f_{\text{IC,pop}}$  for star clusters which all formed in a single starburst. Here, we consider the opposite scenario where star formation proceeds continuously with the SFR constant in

time. The particular value of the SFR is not important as long as it allows us to fully sample the upper limit of the ECMF, because of the normalisation to the total number of stars formed. The results are relevant to stars younger than 300 Myr only because of the duration of our simulations. Such a star formation history produces a time-independent fraction  $\bar{f}_{\text{IC,pop}}(t < 300 \text{ Myr})$  of stars in clusters, which is listed in Table 1.

The first three lines of the table feature star clusters with  $(M_{\text{ecl,min}}, M_{\text{ecl,max}}) = (30 M_{\odot}, 10^4 M_{\odot})$  and  $\beta = 2$ . In these models, we use the same cluster mass range at all the galactocentric radii  $R_g$  to study the influence of the tidal field strength. For these clusters,  $\bar{f}_{\text{IC,pop}}(t < 300 \text{ Myr})$  increases with increasing  $R_g$  from 0.26 for  $R_g = 4 \text{ kpc}$  to 0.41 for  $R_g = 12 \text{ kpc}$ .

There is evidence that the mass of the most massive cluster decreases with the local gas column density (Pflamm-Altenburg & Kroupa 2008). In disc galaxies, the dependence can be approximated as  $\propto \exp(-3R_g/2R_d)$ , where  $R_d$  is the disc scale-length. Taking this dependence into account (with  $R_d = 4 \text{ kpc}$ ), we obtain  $\bar{f}_{\text{IC,pop}}(t < 300 \text{ Myr})$  decreasing with  $R_g$  from 0.36 for  $R_g = 4 \text{ kpc}$  to 0.29 for  $R_g = 12 \text{ kpc}$  (second group of models in Table 1). Thus, the decreasing  $M_{\text{ecl,max}}$  with  $R_g$  acts in the opposite way than the decreasing tidal field strength (as discussed in the previous paragraph), and it has more impact on  $\bar{f}_{\text{IC,pop}}$  than the tidal field.

The third group of records in Table 1 lists the time-averaged fractions of stars in clusters for stars in six different mass bins for clusters with  $R_g = 8 \text{ kpc}$  and  $M_{\text{ecl,max}} = 10^4 M_{\odot}$ . The value of  $\bar{f}_{\text{IC,pop}}(m, t < 300 \text{ Myr})$  increases monotonically with stellar mass from 0.32 for M stars to 0.41 for late B (B3-A0) stars. Stars more massive than that have substantially higher  $\bar{f}_{\text{IC,pop}}(m, t < 300 \text{ Myr})$  (reaching 0.83 for O and early B stars) not only as the result of dynamical mass segregation, but also because they are present only in the youngest clusters, which have had not enough time to dissolve.

The last 15 lines of Table 1 represent the results with the cluster mass limits  $(M_{\text{ecl,min}}, M_{\text{ecl,max}})$  set according to the IGIMF theory (Sect. 4.3). The Table shows the same trend as we encountered in Sect. 4.3:  $\bar{f}_{\text{IC,pop}}(t < 300 \text{ Myr})$  increases with increasing SFR and decreasing  $\beta$ . For models with a top-heavy ECMF ( $\beta = 1.5$ ),  $\bar{f}_{\text{IC,pop}}(t < 300 \text{ Myr})$  strongly depends on the SFR:  $\bar{f}_{\text{IC,pop}}(t < 300 \text{ Myr})$  increases by more than a factor of 2 from  $\bar{f}_{\text{IC,pop}}(t < 300 \text{ Myr}) = 0.39$  for  $\text{SFR} = 0.01 M_{\odot} \text{ yr}^{-1}$  to  $\bar{f}_{\text{IC,pop}}(t < 300 \text{ Myr}) = 0.84$  for  $\text{SFR} = 100 M_{\odot} \text{ yr}^{-1}$ . On the other hand, models with a top-light ECMF ( $\beta = 2.4$ ) have  $\bar{f}_{\text{IC,pop}}(t < 300 \text{ Myr})$  almost independent of SFR because such a steep  $\beta$  ensures that there are very few massive star clusters, which would contribute to a higher  $\bar{f}_{\text{IC,pop}}(t < 300 \text{ Myr})$ .

The model of  $\beta = 2$  and  $\text{SFR} = 1 M_{\odot} \text{ yr}^{-1}$  is close to the Galaxy in the IGIMF framework, which includes the cluster population of the whole Galaxy. This model provides  $\bar{f}_{\text{IC,pop}}(t < 300 \text{ Myr}) = 0.42$ . Since the mass of the most massive cluster decreases with the local gas column density (Pflamm-Altenburg & Kroupa 2008), the majority of the most massive star clusters in the Galaxy are located near the Galactic centre or tips of the bar (Portegies Zwart et al. 2010), and the environment in the vicinity of the Sun hosts

$\beta$	SFR [ $M_{\odot} \text{ yr}^{-1}$ ]	$M_{\text{ecl,min}}$ [ $M_{\odot}$ ]	$M_{\text{ecl,max}}$ [ $M_{\odot}$ ]	Spectral type	$R_{\text{g}}$ [kpc]	$\bar{f}_{\text{IC,pop}}(t < 300 \text{ Myr})$
2.0	-	30	$1.0 \times 10^4$	all	4	0.26
2.0	-	30	$1.0 \times 10^4$	all	8	0.33
2.0	-	30	$1.0 \times 10^4$	all	12	0.41
2.0	-	30	$2.0 \times 10^4$	all	4	0.36
2.0	-	30	$4.0 \times 10^3$	all	8	0.30
2.0	-	30	$1.0 \times 10^3$	all	12	0.29
2.0	-	30	$1.0 \times 10^4$	O-B3	8	0.83
2.0	-	30	$1.0 \times 10^4$	B0-B3	8	0.67
2.0	-	30	$1.0 \times 10^4$	B3-A0	8	0.41
2.0	-	30	$1.0 \times 10^4$	A	8	0.39
2.0	-	30	$1.0 \times 10^4$	F-K	8	0.35
2.0	-	30	$1.0 \times 10^4$	M	8	0.32
1.5	0.01	5	$2.7 \times 10^3$	all	8	0.39
1.5	0.10	5	$1.5 \times 10^4$	all	8	0.55
1.5	1.00	5	$8.5 \times 10^4$	all	8	0.72
1.5	10.00	5	$4.8 \times 10^5$	all	8	0.78
1.5	100.00	5	$2.7 \times 10^6$	all	8	0.84
2.0	0.01	5	$2.7 \times 10^3$	all	8	0.24
2.0	0.10	5	$1.5 \times 10^4$	all	8	0.32
2.0	1.00	5	$8.5 \times 10^4$	all	8	0.42
2.0	10.00	5	$4.8 \times 10^5$	all	8	0.47
2.0	100.00	5	$2.7 \times 10^6$	all	8	0.53
2.4	0.01	5	$2.7 \times 10^3$	all	8	0.16
2.4	0.10	5	$1.5 \times 10^4$	all	8	0.17
2.4	1.00	5	$8.5 \times 10^4$	all	8	0.18
2.4	10.00	5	$4.8 \times 10^5$	all	8	0.19
2.4	100.00	5	$2.7 \times 10^6$	all	8	0.19

**Table 1.** The fraction of stars in clusters  $\bar{f}_{\text{IC,pop}}(t < 300 \text{ Myr})$  for a time independent SFR for stars younger than 300 Myr. The data are divided into four groups as indicated by the horizontal lines. The first group of three rows corresponds to the models of Sect. 4.2 with fixed  $M_{\text{ecl,max}}$ , which are calculated at three different  $R_{\text{g}}$ . The second group is for the same models but assuming  $M_{\text{ecl,max}}$  dependent on the galactocentric radius according to Pflamm-Altenburg & Kroupa (2008). The third group of six rows lists the fraction of stars in clusters according to their spectral type for the models with  $R_{\text{g}} = 8 \text{ kpc}$ . The last group represents the IGIMF models with different ECMF slopes  $\beta$  and SFRs (models of Sect. 4.3). The upper cluster mass limit  $M_{\text{ecl,max}}$  is a function of the assumed SFR (eq. 6).

clusters with masses only up to  $M_{\text{ecl,max}} \approx 4000 M_{\odot}$ . This cluster mass limit provides  $\bar{f}_{\text{IC,pop}}(t < 300 \text{ Myr}) = 0.26$ , which is by  $\approx 40\%$  lower than what we obtain for the Galaxy as a whole.

#### 4.5. Comparison to observations and to the current theoretical model

The observations of Chandar et al. (2017) present results for eight galaxies. We focus particularly on Small and Large Magellanic Clouds, because they differ most from the  $\Gamma$ - $\Sigma_{\text{SFR}}$  model (the two data points with the lowest  $\Sigma_{\text{SFR}}$  in Fig. 5) at their youngest age. These data points utilise the cluster catalogue of Hunter et al. (2003), which is based on visual inspection of cluster candidates from previous catalogues. Hunter et al. (2003) take a candidate object as a cluster if it is distinguishable from the background galaxy within a circle of radius  $23''$  (5.5 pc at the distance of 50 kpc), and resolved at least to several stars. This makes our simulations difficult to be directly compared with observations because we cannot automatically identify star clusters in our simulations based on exactly defined criteria.

To provide an order of magnitude estimate, we place a circle of radius  $r_{\text{search}}$  at the cluster density centre, and count the number of stars located within the projected circle. If at least 10 stars of spectral type A and earlier are found, we consider the cluster to be detected, and we count the stars within radius  $r_{\text{search}}$  as the cluster population, while the rest of the stars count to the field population. Otherwise, we do not consider the cluster to be detected and count all stars in it as the field population. To estimate the sensitivity of this method, we use two radii: 2 pc and 5 pc, the latter one is close to the radius  $\approx 5.5 \text{ pc}$  adopted by Hunter et al. (2003).

Fig. 5 compares the fraction of stars detected by the method described above in our simulations (hatched areas and dashed lines) with the observational data due to Chandar et al. (2017) (empty squares with error bars). The SFR is related to the  $\Sigma_{\text{SFR}}$  on the assumption that each galaxy has a star formation area of  $100 \text{ kpc}^2$ ; this order of magnitude estimate is compatible with the galaxies studied by Chandar et al. (2017) (cf. their table 1). We evaluate  $\bar{f}_{\text{IC,pop}}^{\text{obs}}$  at the same time intervals as the observational data except the oldest age interval, which we take from 100 Myr to 300 Myr, while the observations take it from 100 Myr to 400 Myr. The hatched areas cover the



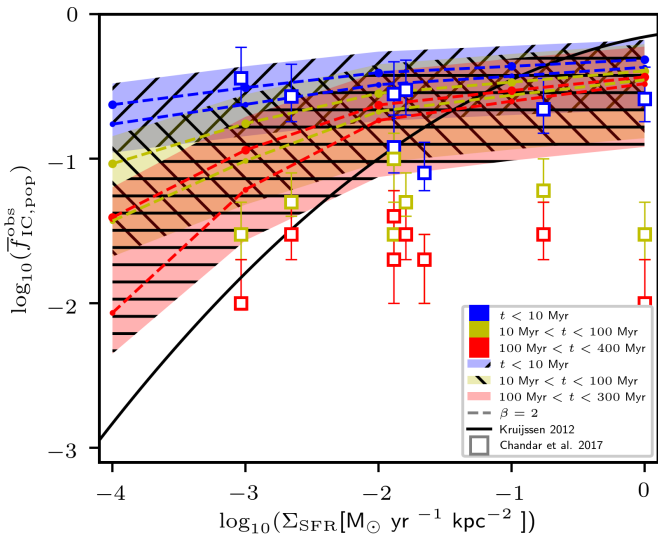


**Fig. 5.** The likely detected fraction of stars in clusters of age  $t < 10$  Myr (blue area and blue lines),  $10 \text{ Myr} < t < 100$  Myr (yellow area and yellow lines), and  $100 \text{ Myr} < t < 300$  Myr (red area and red lines) as a function of  $\Sigma_{\text{SFR}}$ . Apart from indicating age by a colour, age is also shown by a hatch style. The coloured area is bordered by two extreme models: the lower one has  $\beta = 2.2$  and  $r_{\text{search}} = 2$  pc, the upper one has  $\beta = 1.8$  and  $r_{\text{search}} = 5$  pc. The models for  $\beta = 2.0$  and  $r_{\text{search}} = 2$  pc and  $5$  pc are shown by the dashed lines. The plot shows how  $\bar{f}_{\text{IC,pop}}^{\text{obs}}$  increases with the  $\Sigma_{\text{SFR}}$ , and how it decreases with the cluster age. The observational data due to Chandar et al. (2017), which aim consistently at galaxies both with low SFR and high SFR, are shown by empty squares with their errorbars. Our results are obtained at almost the same time intervals as the observational data (indicated by the colours). The semi-analytic estimate provided by the  $\Gamma$ - $\Sigma_{\text{SFR}}$  model is shown by the black solid line. Note its disagreement with the observational data for the clusters of any age interval.

range of  $\beta \in (1.8, 2.2)$  and  $r_{\text{search}}$  between 2 and 5 pc, while the dashed lines show the value of  $\bar{f}_{\text{IC,pop}}^{\text{obs}}$  for  $\beta = 2$  and  $r_{\text{search}} = 2$  pc and 5 pc. The youngest clusters (blue symbols and lines; age  $< 10$  Myr) have  $\bar{f}_{\text{IC,pop}}^{\text{obs}}$  comparable to observations, while older clusters have  $\bar{f}_{\text{IC,pop}}^{\text{obs}}$  higher than in observations. Thus, the rough approximation to 'synthetic observations' is in agreement with the original hypothesis that all stars originate in gravitationally bound embedded clusters. Gas expulsion not only unbinds many stars from the clusters, but also decreases their density so that many of the youngest clusters cannot be detected, an idea originally proposed by Lüghausen et al. (2012). The overestimate of  $\bar{f}_{\text{IC,pop}}^{\text{obs}}$  in older clusters can be caused by neglecting the interaction of clusters with molecular clouds in our models, which probably plays an important role in cluster dissolution (Terlevich 1987; Lamers & Gieles 2006; Chandar et al. 2010; Jerabkova et al. 2021).

Only the youngest objects can be compared with the  $\Gamma$ - $\Sigma_{\text{SFR}}$  theory because the theory does not consider any process which releases stars after the clusters emerge from their natal clouds, which occurs at the age of several Myr. This constrains the comparison to the youngest objects (10 Myr; blue lines and squares in Fig. 5), which are the least impacted by dynamical evolution. Thus,  $\Gamma \approx \bar{f}_{\text{IC,pop}}(t < 10 \text{ Myr})$ . For low SFRs,  $\Gamma$ -1 models predict substantially

larger values of  $\bar{f}_{\text{IC,pop}}^{\text{obs}}(t < 10 \text{ Myr})$  in contrast to the  $\Gamma$ - $\Sigma_{\text{SFR}}$  model: for  $\Sigma_{\text{SFR}} = 10^{-4} M_{\odot} \text{ yr}^{-1} \text{ kpc}^{-2}$ , the admitted values of  $\bar{f}_{\text{IC,pop}}^{\text{obs}}(t < 10 \text{ Myr})$  in  $\Gamma$ -1 models range from 0.07 to 0.45, while the  $\Gamma$ - $\Sigma_{\text{SFR}}$  model predicts  $\Gamma = 0.0015$ .<sup>3</sup> For high SFRs, the  $\Gamma$ -1 model predicts lower  $\bar{f}_{\text{IC,pop}}^{\text{obs}}(t < 10 \text{ Myr})$  in contrast to the  $\Gamma$ - $\Sigma_{\text{SFR}}$  model.

In the  $\Gamma$ - $\Sigma_{\text{SFR}}$  model as well as in the  $\Gamma$ -1 model,  $\Gamma$  increases with  $\Sigma_{\text{SFR}}$ . However, the reason for this behaviour is very different. In the  $\Gamma$ - $\Sigma_{\text{SFR}}$  model, it is the combined effect of the increasing SFE( $x$ ) and  $\gamma(x)$  with  $x$ , where high values of  $x$  are reached as the ISM probability distribution function widens with increasing  $\rho_{\text{ISM}}$  (via the ISM Mach number). In contrast, in the  $\Gamma$ -1 model, the increase is due to the expansion and partial dissolution of clusters as the result of gas expulsion, which has a lesser impact on more massive clusters, which according to the IGIMF theory form only in galaxies with a sufficiently high  $\Sigma_{\text{SFR}}$ . Another difference is the much weaker dependence of  $\Gamma$  on  $\Sigma_{\text{SFR}}$ , which was noted by Chandar et al. (2017), and which is reproduced in the  $\Gamma$ -1 model.

## 5. Discussion

### 5.1. The influence of the initial conditions of star clusters

To calculate the present models, we adopt particular initial conditions, which are described in Sect. 3.1.1. However, both observational and theoretical evidence indicate that the initial conditions for star cluster formation are not fully understood. For example, the value of the SFE, initial cluster radii, the time-scale of gas expulsion and the degree of primordial mass segregation are subject to ongoing research (e.g. Er et al. 2013; Kuhn et al. 2014; Banerjee & Kroupa 2015; Megeath et al. 2016; Spera & Capuzzo-Dolcetta 2017; Domínguez et al. 2017; Pfalzner 2019; Kuhn et al. 2019; Dib & Henning 2019; Pang et al. 2020). Some of the cluster initial conditions are interrelated: for example, embedded star clusters cannot form with sub-parsec scales and SFE close to 100% because they would not be able to expand to their observed sizes (Banerjee & Kroupa 2017).

#### 5.1.1. Initial cluster radius and the SFE

To study the possible influence of the initial cluster radius and the SFE, we perform additional models with clusters of slightly larger radii (by at most a factor of 3; "A" models) and clusters of a slightly lower SFE of 0.25 ("F" models) (see Sect. 3.1.2 for the model descriptions). The time dependence of  $f_{\text{IC}}(M_{\text{ecl}})$  for clusters of four different masses is shown in Fig. 6. In comparison to the standard models ("S" models), both "A" and "F" models release stars to the field earlier, and have a faster cluster dissolution. Also, the most massive clusters in our sample (6400  $M_{\odot}$ ) have lost most of their stars already by 30 Myr in "A" and "F" models, while

<sup>3</sup> We note that we compare the 'observed' fraction of stars in clusters in the  $\Gamma$ -1 model (i.e.  $\bar{f}_{\text{IC,pop}}^{\text{obs}}(t < 10 \text{ Myr})$ ) with the physical fraction (i.e.  $\Gamma$ ) of the  $\Gamma$ - $\Sigma_{\text{SFR}}$  model. However, the observed fraction of stars in clusters is always lower than the physical fraction (i.e.,  $\bar{f}_{\text{IC,pop}}^{\text{obs}}(t < 10 \text{ Myr}) < \bar{f}_{\text{IC,pop}}(t < 10 \text{ Myr})$ ) because of incompleteness, which makes the difference with the  $\Gamma$ - $\Sigma_{\text{SFR}}$  model even more pronounced.

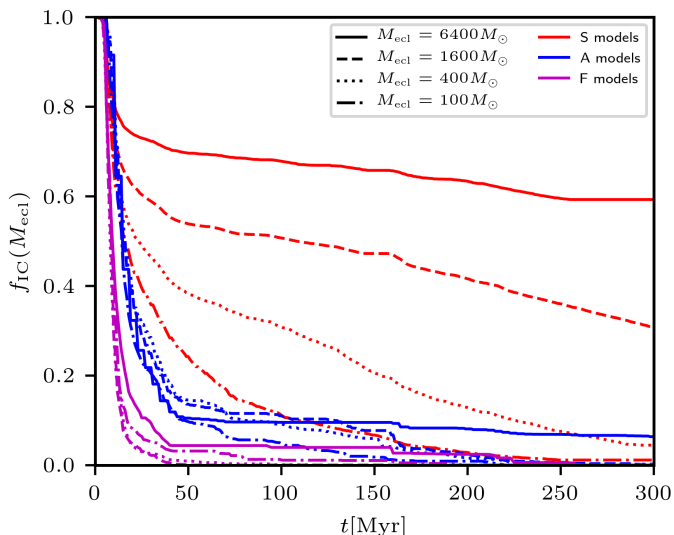


**Fig. 6.** The fraction of stars located in clusters of an initial mass  $M_{\text{ecl}}$  for "A" models (blue lines) and "F" models (magenta lines). For comparison, standard models are shown by red lines. "A" and "F" models result in substantially lower fraction of stars in clusters of all considered masses at  $t \geq 20$  Myr.

the clusters are relatively unaffected in the standard models even at 300 Myr.

For a Milky Way-like galaxy with constant star formation rate and star formation parameters  $\beta = 2$  and  $\text{SFR} = 1 M_{\odot} \text{ yr}^{-1}$ , "A" and "F" models have only  $\bar{f}_{\text{IC, pop}}(t < 300 \text{ Myr}) = 0.11$  and  $0.06$ , respectively, while it is  $0.42$  in standard models. The difference of  $\bar{f}_{\text{IC, pop}}$  between the models is small in the youngest clusters, but it gets pronounced with time. Model "A" has the interesting property of  $\bar{f}_{\text{IC, pop}}(M_{\text{ecl}})$  being almost independent of the cluster mass by  $\approx 150$  Myr for the cluster mass range spanning more than one order of magnitude from  $\approx 400 M_{\odot}$  to  $\approx 6400 M_{\odot}$ . This property is not seen in models "F" and "S", which have a smaller cluster radii. This behaviour is in line with the observations indicating that the dissolution rate of star clusters is independent of their initial mass (e.g. Lada & Lada 2003; Fall et al. 2005; Whitmore et al. 2007), but such an explanation is only hypothetical for now given the model uncertainties and the uncertain role of molecular clouds in cluster dissolution.

The physical reason for the faster release of stars from clusters in the "A" models is due to gas expulsion occurring more impulsively, i.e. the ratio between the gas expulsion time-scale and the cluster crossing time,  $\tau_{\text{M}}/t_{\text{cross}}$ , being smaller. Since  $\tau_{\text{M}}/t_{\text{cross}} \propto \sqrt{M_{\text{ecl}}/a_{\text{ecl}}}$  and  $a_{\text{ecl}} \propto M_{\text{ecl}}^{1/3}$ , the difference between the "A" and "S" models increases with increasing cluster mass. The impact of gas expulsion increases strongly when  $\tau_{\text{M}}/t_{\text{cross}}$  becomes smaller than unity (Baumgardt & Kroupa 2007), which is the case of all clusters in the "A" models. The most massive clusters ( $M_{\text{ecl}} = 6400 M_{\odot}$ ) have  $\tau_{\text{M}}/t_{\text{cross}} = 1$  for "S" models, while it is  $0.63$  for "A" models. Because of the monotonic increase of the ratio  $\tau_{\text{M}}/t_{\text{cross}}$  with  $M_{\text{ecl}}$  (as  $M_{\text{ecl}}^{1/3}$  for "A" models), clusters with  $M_{\text{ecl}} < 6400 M_{\odot}$  have  $\tau_{\text{M}}/t_{\text{cross}} < 0.63$ , resulting in their rapid dissolution. The reason for the faster release of stars from clusters in "F" models is due to their lower SFE (Baumgardt & Kroupa 2007).

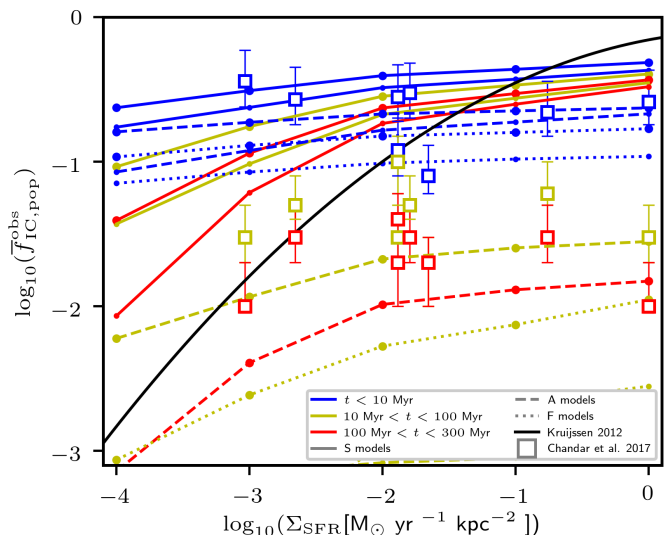


**Fig. 7.** The fraction of stars which is likely to be observed in clusters of age  $t < 10$  Myr (blue lines),  $10 \text{ Myr} < t < 100 \text{ Myr}$  (yellow lines), and  $100 \text{ Myr} < t < 300 \text{ Myr}$  (red lines) as a function of  $\Sigma_{\text{SFR}}$ . The plot shows results for "S", "A" and "F" models for the ECMF of slope  $\beta = 2$  by solid, dashed and dotted lines, respectively. The lines are shown for  $r_{\text{search}} = 2 \text{ pc}$  (smaller dots) and  $r_{\text{search}} = 5 \text{ pc}$  (larger dots) for each model. The prediction of the  $\Gamma$ - $\Sigma_{\text{SFR}}$  model and the observational data due to Chandar et al. (2017) are shown by the black line and by squares, respectively.

Figure 7 shows the fraction of stars which is likely to be observed in clusters for the "S", "A" and "F" models assuming the IGIMF theory and  $\beta = 2$ . For the youngest clusters ( $t \lesssim 10$  Myr; blue lines), the difference between the models varies less than by a factor of three; it decreases from  $\bar{f}_{\text{IC, pop}}^{\text{obs}}(t < 10 \text{ Myr}) \approx 0.35$  for S models to  $\bar{f}_{\text{IC, pop}}^{\text{obs}}(t < 10 \text{ Myr}) \approx 0.13$  for F models (for Milky Way-like  $\Sigma_{\text{SFR}}$  of  $\approx 1 M_{\odot} \text{ yr}^{-1}$ ). Similar to the "S" models, both "A" and "F" models reasonably agree with the observations, and they show a much weaker dependence on  $\Sigma_{\text{SFR}}$  than predicted by the  $\Gamma$ - $\Sigma_{\text{SFR}}$  theory.

For older clusters (age  $\geq 10$  Myr; yellow and red lines in Fig. 7), "A" and "F" models result in significantly lower observed fractions of stars in clusters than in the standard model. This brings "A" and "F" models closer to the observations of Chandar et al. (2017) also at later times; the modelled values of  $\bar{f}_{\text{IC, pop}}^{\text{obs}}(10 \text{ Myr} < t < 100 \text{ Myr})$  and  $\bar{f}_{\text{IC, pop}}^{\text{obs}}(t < 300 \text{ Myr})$  are even lower than the observations. "F" models have a too low fraction of stars in clusters. This indicates that the observational data could be well reproduced also for clusters older than 10 Myr and as old as at least 300 Myr by either steepening the relationship between the cluster mass and its radius, or by lowering the SFE (albeit the latter possibility needs the SFE somewhere between  $0.25$  and  $0.33$ ) without considering any additional cluster dissolving mechanism such as interactions with molecular clouds. This is a remarkable property of "A" and "F" models because standard models necessitate an additional cluster dissolving mechanism to explain the observations for  $t \geq 10$  Myr (Sect. 4.5). Given the large sensitivity of the fraction of stars in clusters on the SFE and possibly  $\tau_{\text{M}}$ , it is probable that the observations for clusters

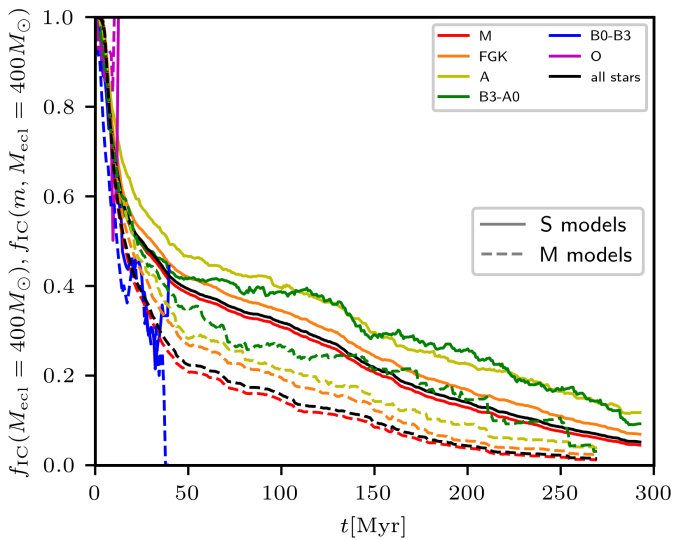


**Fig. 8.** The time dependence of  $f_{\text{IC}}(m)$  for clusters of mass  $400 M_{\odot}$  starting with initial conditions for models "S" (solid lines), and "M" (dashed lines). The values of  $f_{\text{IC}}(m)$  for different stellar spectral types is shown by line colours. The fraction of all stars in clusters  $f_{\text{IC}}(M_{\text{ecl}} = 400 M_{\odot})$  is shown by the black lines. The clusters orbit the galaxy at  $R_{\text{g}} = 8$  kpc, and they have metallicity  $Z = 0.014$ .

up to the age of at least 300 Myr can be explained by more combinations of the cluster parameters ( $a_{\text{ecl}}$ , SFE and  $\tau_{\text{M}}$ ) than considered in this work.

The impact of gas expulsion on a cluster is a strong function of the ratio  $\tau_{\text{M}}/t_{\text{cross}}$  (Lada et al. 1984; Baumgardt & Kroupa 2007). For all the clusters studied in this work, gas expulsion is impulsive ( $\tau_{\text{M}}/t_{\text{cross}} \lesssim 1$ ). Assuming  $\tau_{\text{M}} = 10 \text{ km s}^{-1}$  independent of  $M_{\text{ecl}}$ , gas expulsion becomes adiabatic ( $\tau_{\text{M}}/t_{\text{cross}} \gg 1$ ) if  $M_{\text{ecl}} \gg 10^4 M_{\odot}$ . Adiabatic gas expulsion unbinds a substantially lower fraction of stars than impulsive gas expulsion (e.g. Lada et al. 1984). Since we extrapolate results from clusters with impulsive gas expulsion towards the more massive ones with adiabatic gas expulsion,  $f_{\text{IC}}(M_{\text{ecl}})$  is underestimated for  $M_{\text{ecl}} \gtrsim 10^4 M_{\odot}$ . We estimate that this effect is of secondary importance (at least for the clusters in the youngest age bin) because  $f_{\text{IC}}(M_{\text{ecl}} = 6400 M_{\odot}) \gtrsim 0.8$  (Fig. 1). Even if  $f_{\text{IC}}(M_{\text{ecl}})$  were 1 for  $M_{\text{ecl}} \gtrsim 10^4 M_{\odot}$ ,  $\bar{f}_{\text{IC, pop}}^{\text{obs}}(t < 10 \text{ Myr})$  cannot differ by more than a factor of  $1/0.8 = 1.25$  from the present models.

The models with SFE = 0.25 present a lower estimate on the SFE because they underestimate the fractions of stars in clusters after 10 Myr (Fig. 7). What is the expected fraction of stars in clusters in the other extreme if we consider an absence of gas expulsion (i.e. SFE = 1)? In this case, the clusters would be unaffected, so they would resemble their state at  $t = 0$ , at which time  $\bar{f}_{\text{IC, pop}}^{\text{obs}}(0) = 0.61$  for a Milky Way-like galaxy ( $\Sigma_{\text{g}} = 1 M_{\odot} \text{ pc}^{-2}$  and  $\beta = 2$ ). The present simulations predict  $\bar{f}_{\text{IC, pop}}^{\text{obs}}(t < 10 \text{ Myr}) \approx 0.35$ . Thus, the uncertainty in gas expulsion parameters can increase the value of  $\bar{f}_{\text{IC, pop}}^{\text{obs}}(t < 10 \text{ Myr})$  by at most a factor of 1.8.

### 5.1.2. Primordial mass segregation

To study the possible influence of the initial conditions on the fraction of stars to be found in clusters, we perform additional models with a high degree of primordial mass segregation (models "M"), which are detailed in Sect. 3.1.2. These models present likely the extreme cases of stellar concentrations within the clusters, having a very compact core of massive stars, while the standard ("S" models) are of a more uniform density. Figure 8 compares the time dependence of  $f_{\text{IC}}(m)$  for a cluster of mass  $400 M_{\odot}$  between "S" and "M" models.

Generally, all the models have  $f_{\text{IC}}(m)$  increasing with  $m$  at a given time, which reflects mass segregation, which establishes dynamically in models "S". The primordially mass segregated clusters "M" lose stars more quickly and dissolve earlier than their non-mass segregated counterparts "S". Assuming that we observe clusters of mass  $400 M_{\odot}$ , which formed in a galaxy with a constant SFR over a long time interval (longer than  $\sim 300 \text{ Myr}$ ), the fraction of stars found in these clusters is  $\bar{f}_{\text{IC}}(t < 300 \text{ Myr}) = 0.26$  for "S" models and  $\bar{f}_{\text{IC}}(t < 300 \text{ Myr}) = 0.17$  for "M" models. These values are for all stars in gravitationally bound objects, many of which are comprised from only tens of stars, and are not likely to be observed. The same estimate of the fraction of observable stars in clusters as done in Sect. 4.5 yields for "S" models  $\bar{f}_{\text{IC}}^{\text{obs}}(t < 10 \text{ Myr}) = 0.34$  and  $\bar{f}_{\text{IC}}^{\text{obs}}(t < 10 \text{ Myr}) = 0.49$  for  $r_{\text{search}} = 2 \text{ pc}$  and  $5 \text{ pc}$ , respectively. "M" models have slightly lower fractions of the youngest stars in clusters,  $\bar{f}_{\text{IC}}^{\text{obs}}(t < 10 \text{ Myr}) = 0.31$  and  $\bar{f}_{\text{IC}}^{\text{obs}}(t < 10 \text{ Myr}) = 0.48$  for  $r_{\text{search}} = 2 \text{ pc}$  and  $5 \text{ pc}$ , respectively. Thus, primordial mass segregation decreases  $\bar{f}_{\text{IC}}$  in a population of clusters, but its observed manifestation in the youngest age group is modest.

We expect that the difference of  $\bar{f}_{\text{IC}}^{\text{obs}}(t < 10 \text{ Myr})$  between "M" and "S" models decreases for clusters more massive than  $400 M_{\odot}$  because more massive clusters tend to retain more of their stars, and the difference increases for clusters of mass below  $400 M_{\odot}$  for the opposite reason<sup>4</sup>. In total, we expect that for a population of primordially mass segregated clusters with  $\beta = 2$ ,  $\bar{f}_{\text{IC}}^{\text{obs}}(t < 10 \text{ Myr})$  is slightly lower (approximately up to a factor of 1.2) than for the non-mass segregated clusters.

### 5.2. The influence of the form of the ECMF

The admitted variation of the slope  $\beta$ , which ranges from 1.8 to 2.2 in most galaxies (e.g. Whitmore et al. 1999; Lada & Lada 2003; Chandar et al. 2010), results in the 'observed' variation of the fraction of stars in the youngest clusters to vary in the range of  $\bar{f}_{\text{IC}}^{\text{obs}}(t < 10 \text{ Myr}) = 0.18$  to  $0.55$  (for a Milky Way-like galaxy with  $\Sigma_{\text{g}} = 1 M_{\odot} \text{ pc}^{-2}$ ). It differs by a factor of 2 from the standard value for  $\beta = 2$ . This uncertainty is of a comparable magnitude as the uncertainty in the initial cluster conditions.

<sup>4</sup> We choose the cluster mass to be  $400 M_{\odot}$  because it lies approximately in between the interval  $(\log_{10}(M_{\text{ecl, min}}), \log_{10}(M_{\text{ecl, max}}))$ , i.e. the total number of stars contained in clusters forming within mass interval  $(M_{\text{ecl, min}}, 400 M_{\odot})$  and  $(400 M_{\odot}, M_{\text{ecl, max}})$  is comparable (assuming  $\beta \approx 2$ ).

Another important parameter of the ECMF is the cluster lower mass limit  $M_{\text{ecl},\text{min}}$ . Chandar et al. (2017) use  $M_{\text{ecl},\text{min}} = 100 M_{\odot}$ , while the formation of clusters of mass significantly lower than that is known (e.g. Kroupa & Bouvier 2003; Kirk & Myers 2011; Joncour et al. 2018; Plunkett et al. 2018). Decreasing the lower mass cluster limit results in a higher value of  $\Gamma$ . For example, for the LMC Chandar et al. (2017) obtain  $\Gamma = 0.27$ , while it would be  $\Gamma = 0.41$  for  $M_{\text{ecl},\text{min}} = 5 M_{\odot}$ . Taking into account a lower mass limit  $M_{\text{ecl},\text{min}}$  would bring their observations to a better agreement with our models.

### 5.3. Comparison to observations

An important step in determining the value of  $\Gamma$  is to identify all clusters above a given mass limit  $M_{\text{ecl},\text{lim}}$  (typically  $M_{\text{ecl},\text{lim}} > M_{\text{ecl},\text{min}}$ ; Goddard et al. 2010; Chandar et al. 2017). Then, the total cluster population is obtained by extrapolating the number of clusters towards  $M_{\text{ecl}}$  lower than  $M_{\text{lim}}$  assuming an ECMF slope  $\beta$ . Even clusters with mass above  $M_{\text{ecl},\text{lim}}$  suffer from incompleteness mainly due to extinction, where some clusters are obscured by molecular clouds, and crowding in the most active star forming regions. These observational limitations tend to underestimate  $\Gamma$ . Taking this into account could improve the agreement between our model and observations in galaxies with higher SFRs as seen in Fig. 5.

## 6. Conclusions

We have investigated whether the majority of stars form in gravitationally bound or unbound systems using N-body simulations. As a starting hypothesis, we assumed that  $\Gamma = 1$ , that is, that all stars form in gravitationally bound embedded clusters. This hypothesis is consistent with and motivated by observational data of young star forming regions. The clusters experience a gravitational potential drop as the result of early gas expulsion, which impacts low-mass clusters more strongly than higher-mass clusters. Additional stars escape their initial host clusters due to ejection, evaporation and the tidal field of the host galaxy.

The time evolution of the fraction of stars in clusters for all clusters originating in a single coeval star burst is shown in Fig. 4. For example, in a Milky Way-like galaxy (SFR  $\approx 1 M_{\odot} \text{ yr}^{-1}$ ) with the ECMF slope  $\beta = 2$ , our simulations predict that 35 % of stars remain gravitationally bound to their initial host clusters at the age of 200 Myr. More massive stars are more likely to be present in clusters (83% of O-type stars) than lower-mass stars (32% of M-type stars younger than 300 Myr; Table 1).

The galactic tidal field disrupts clusters more easily at smaller galactocentric distances  $R_g$ ; assuming the same upper cluster mass limit throughout the galaxy, the fraction of stars in clusters increases by a factor of 1.6 between  $R_g = 4 \text{ kpc}$  and  $R_g = 12 \text{ kpc}$  for  $\beta = 2$  (Table 1). However, in a more realistic scenario where the upper cluster mass limit decreases with increasing  $R_g$ , the fraction of stars in clusters decreases by a factor of 1.2 from  $R_g = 4 \text{ kpc}$  to  $R_g = 12 \text{ kpc}$ , therefore more than compensating for the impact of the tidal field. The influence of cluster metallicity is negligible. If clusters form primordially mass segregated, the fraction of stars in clusters is slightly lower, but not likely more than by a factor of 1.2.

We compare our simulations to observations. This comparison is deemed approximate because of the systematic differences in detecting star clusters and their member stars observationally vs. within our simulations. For the youngest stars ( $t < 10 \text{ Myr}$ ), our models are in agreement with most of the observational data of Chandar et al. (2017) (Fig. 5). Thus, the observations are in agreement with the hypothesis that all stars form in gravitationally bound embedded clusters. We further find a rather weak dependence of the fraction  $\bar{f}_{\text{IC},\text{pop}}^{\text{obs}}(t < 10 \text{ Myr})$  of the observed youngest stars in clusters on  $\Sigma_{\text{SFR}}$ , which contrasts with the strong dependence posited by the  $\Gamma$ - $\Sigma_{\text{SFR}}$  model (Kruijssen 2012). These results show only weak sensitivity on the particular choice of parameters for our model such as the initial cluster radius or the SFE. The physical reason for the dependence of  $\bar{f}_{\text{IC},\text{pop}}^{\text{obs}}$  on  $\Sigma_{\text{SFR}}$  is different from the dependence in the  $\Gamma$ - $\Sigma_{\text{SFR}}$  model: in our model, it is due to the lesser impact of gas expulsion on more massive clusters, which form predominantly in galaxies with higher  $\Sigma_{\text{SFR}}$ , whereas it is due to star formation at higher gas densities, higher SFEs, and higher fraction of stars forming in bound clusters in the  $\Gamma$ - $\Sigma_{\text{SFR}}$  model.

At later times (ages between 10 to 100 Myr and 100 to 300 Myr; Fig. 5), our standard models have too large  $\bar{f}_{\text{IC},\text{pop}}^{\text{obs}}$  compared to observations. A similar result was previously found by Lamers et al. (2005), who did not include early gas expulsion. Thus, early gas expulsion does not reconcile this discrepancy, and other mechanisms (e.g. encounters with giant molecular clouds) are needed to reduce the number of clusters and bring them closer to the observed values. A case in point are the nearby Hyades star cluster, which may be in the process of being disrupted (Jerabkova et al. 2021).

We propose an alternative explanation to this picture. The difference between N-body models and observations could be reconciled by adjusting some parameters of our models (Sect. 5.1.1), the most attractive of which is the SFE and the relationship between the cluster half-mass radius and cluster mass. In this case gas expulsion, cluster dynamics and galactic potential alone bring the results close to observations (at least for clusters younger than 300 Myr) without the necessity of employing additional cluster dissolution mechanisms.

We contrast the dynamical paradigm where all stars form in embedded clusters with the theoretical  $\Gamma$ - $\Sigma_{\text{SFR}}$  framework that derives the functional form of  $\Gamma(\Sigma_{\text{SFR}})$  by combining the observed and modelled properties of the ISM and star forming regions. We identify several questionable points in the  $\Gamma$ - $\Sigma_{\text{SFR}}$  theory, particularly the substitution of several equations into one another, some of which are non-linear and/or contain uncertain or poorly constrained terms. Additionally, the  $\Gamma$ - $\Sigma_{\text{SFR}}$  framework neglects early stellar feedback, Larson's relations, the time-dependent star formation rate during cluster formation, stellar dynamics, and the density threshold for star formation. Using a toy model, we show (in Sect. 2.2) that even small changes (consistent with observations) to the equations assumed by the  $\Gamma$ - $\Sigma_{\text{SFR}}$  model result in very different functional forms of  $\Gamma$  as a function of  $\Sigma_{\text{SFR}}$ . This leads us to challenge the key prediction of the  $\Gamma$ - $\Sigma_{\text{SFR}}$  model: that most stars form as not gravitationally bound to embedded star clusters in Milky Way-like galaxies. Instead, we suggest that cluster dynamics, early gas expulsion, and the influ-

ence of realistic galactic environments (potential and giant molecular clouds) provide an explanation for the fraction of stars observed in star clusters under the hypothesis that all stars originate from gravitationally bound systems.

*Acknowledgements.* We would like to thank an anonymous referee for useful comments, which significantly improved the paper. We thank Sverre Aarseth for continuously developing the code NBODY6 as well as for his numerous pieces of advice. FD acknowledges the European Southern Observatory in Garching where part of this work was completed under the Scientific Visitors Programme. PK acknowledges support from the Grant Agency of the Czech Republic under grant number 20-21855S. RIA acknowledges funding provided by an SNSF Eccellenza Professorial Fellowship (Grant No. PCEFP2\_194638) and funding from the European Research Council (ERC) under the European Union's Horizon 2020 research and innovation programme (Grant Agreement No. 947660). We appreciate the support of the ESO IT team, which was vital for performing the presented numerical models. This research made use of Matplotlib Python Package (Hunter 2007).

## References

- Aarseth, S. J. 2003, *Gravitational N-Body Simulations* (Cambridge: Cambridge University Press)
- Aarseth, S. J. & Zare, K. 1974, *Celestial Mechanics*, 10, 185
- Adamo, A., Östlin, G., & Zackrisson, E. 2011, *MNRAS*, 417, 1904
- Ahmad, A. & Cohen, L. 1973, *Journal of Computational Physics*, 12, 389
- Allen, C. & Santillan, A. 1991, *Rev. Mexicana Astron. Astrofís.*, 22, 255
- Alves, J., Lombardi, M., & Lada, C. J. 2007, *A&A*, 462, L17
- André, P., Di Francesco, J., Ward-Thompson, D., et al. 2014, in *Protostars and Planets VI*, ed. H. Beuther, R. S. Klessen, C. P. Dullemond, & T. Henning, 27
- Banerjee, S. & Kroupa, P. 2013, *ApJ*, 764, 29
- Banerjee, S. & Kroupa, P. 2015, *MNRAS*, 447, 728
- Banerjee, S. & Kroupa, P. 2017, *A&A*, 597, A28
- Baumgardt, H. & Kroupa, P. 2007, *MNRAS*, 380, 1589
- Baumgardt, H. & Makino, J. 2003, *MNRAS*, 340, 227
- Bik, A., Lamers, H. J. G. L. M., Bastian, N., Panagia, N., & Romaniello, M. 2003, *A&A*, 397, 473
- Blaauw, A. 1964, *ARA&A*, 2, 213
- Boily, C. M. & Kroupa, P. 2003, *MNRAS*, 338, 673
- Bonnell, I. A., Bate, M. R., Clarke, C. J., & Pringle, J. E. 1997, *MNRAS*, 285, 201
- Bonnell, I. A., Bate, M. R., Clarke, C. J., & Pringle, J. E. 2001, *MNRAS*, 323, 785
- Bonnell, I. A., Bate, M. R., & Zinnecker, H. 1998, *MNRAS*, 298, 93
- Bressert, E., Bastian, N., Gutermuth, R., et al. 2010, *MNRAS*, 409, L54
- Carpenter, J. M. 2000, *AJ*, 120, 3139
- Carpenter, J. M., Snell, R. L., & Schloerb, F. P. 1995, *ApJ*, 450, 201
- Chandar, R., Fall, S. M., & Whitmore, B. C. 2010, *ApJ*, 711, 1263
- Chandar, R., Fall, S. M., Whitmore, B. C., & Mulia, A. J. 2017, *ApJ*, 849, 128
- Chen, H. H.-H., Burkhardt, B., Goodman, A., & Collins, D. C. 2018, *ApJ*, 859, 162
- Clark, P. C., Bonnell, I. A., Zinnecker, H., & Bate, M. R. 2005, *MNRAS*, 359, 809
- Colín, P., Vázquez-Semadeni, E., & Gómez, G. C. 2013, *MNRAS*, 435, 1701
- de la Fuente Marcos, R. & de la Fuente Marcos, C. 2004, *New A*, 9, 475
- Dib, S. & Henning, T. 2019, *A&A*, 629, A135
- Dinnbier, F. & Walch, S. 2020, *MNRAS*, 499, 748
- Domínguez, R., Fellhauer, M., Blaña, M., Farias, J. P., & Dabringhausen, J. 2017, *MNRAS*, 472, 465
- Elmegreen, B. G. 1983, *MNRAS*, 203, 1011
- Elmegreen, B. G. 2000, *ApJ*, 539, 342
- Elmegreen, B. G., Elmegreen, D. M., Chandar, R., Whitmore, B., & Regan, M. 2006, *ApJ*, 644, 879
- Er, X.-Y., Jiang, Z.-B., & Fu, Y.-N. 2013, *Research in Astronomy and Astrophysics*, 13, 277
- Fall, S. M., Chandar, R., & Whitmore, B. C. 2005, *ApJ*, 631, L133
- Fensch, J., Duc, P.-A., Boquien, M., et al. 2019, *A&A*, 628, A60
- Fujii, M. S. & Portegies Zwart, S. 2011, *Science*, 334, 1380
- Gavagnin, E., Bleuler, A., Rosdahl, J., & Teyssier, R. 2017, *MNRAS*, 472, 4155
- Geen, S., Watson, S. K., Rosdahl, J., et al. 2018, *MNRAS*, 481, 2548
- Geyer, M. P. & Burkert, A. 2001, *MNRAS*, 323, 988
- Gieles, M., Larsen, S. S., Bastian, N., & Stein, I. T. 2006, *A&A*, 450, 129
- Goddard, Q. E., Bastian, N., & Kennicutt, R. C. 2010, *MNRAS*, 405, 857
- González-Samaniego, A. & Vázquez-Semadeni, E. 2020, *MNRAS*, 499, 668
- Goodwin, S. P. 1997, *MNRAS*, 284, 785
- Goodwin, S. P., Nutter, D., Kroupa, P., Ward-Thompson, D., & Whitworth, A. P. 2008, *A&A*, 477, 823
- Gvaramadze, V. V., Weidner, C., Kroupa, P., & Pflamm-Altenburg, J. 2012, *MNRAS*, 424, 3037
- Haid, S., Walch, S., Seifried, D., et al. 2018, *MNRAS*, 478, 4799
- Heiderman, A., Evans, Neal J., I., Allen, L. E., Huard, T., & Heyer, M. 2010, *ApJ*, 723, 1019
- Heyer, M., Krawczyk, C., Duval, J., & Jackson, J. M. 2009, *ApJ*, 699, 1092
- Hunter, D. A., Elmegreen, B. G., Dupuy, T. J., & Mortonson, M. 2003, *AJ*, 126, 1836
- Hunter, J. D. 2007, *Computing in Science & Engineering*, 9, 90
- Hurley, J. R., Pols, O. R., & Tout, C. A. 2000, *MNRAS*, 315, 543
- Hurley, J. R., Tout, C. A., & Pols, O. R. 2002, *MNRAS*, 329, 897
- Jerabkova, T., Boffin, H. M. J., Beccari, G., et al. 2021, *A&A*, 647, A137
- Jeřábková, T., Hasani Zonoozi, A., Kroupa, P., et al. 2018, *A&A*, 620, A39
- Johnson, L. C., Seth, A. C., Dalcanton, J. J., et al. 2016, *ApJ*, 827, 33
- Johnson, L. C., Seth, A. C., Dalcanton, J. J., et al. 2017, *ApJ*, 839, 78
- Joncour, I., Duchêne, G., Moraux, E., & Motte, F. 2018, *A&A*, 620, A27
- Kennicutt, Robert C., J. 1998, *ApJ*, 498, 541
- Kirk, H. & Myers, P. C. 2011, *ApJ*, 727, 64
- Kritsuk, A. G., Norman, M. L., & Wagner, R. 2011, *ApJ*, 727, L20
- Kroupa, P. 1995a, *MNRAS*, 277, 1491
- Kroupa, P. 1995b, *MNRAS*, 277, 1507
- Kroupa, P. 2001, *MNRAS*, 322, 231
- Kroupa, P., Aarseth, S., & Hurley, J. 2001, *MNRAS*, 321, 699
- Kroupa, P. & Bouvier, J. 2003, *MNRAS*, 346, 343
- Kroupa, P. & Weidner, C. 2003, *ApJ*, 598, 1076
- Kruijssen, J. M. D. 2012, *MNRAS*, 426, 3008
- Kuhn, M. A., Feigelson, E. D., Getman, K. V., et al. 2014, *ApJ*, 787, 107
- Kuhn, M. A., Hillenbrand, L. A., Sills, A., Feigelson, E. D., & Getman, K. V. 2019, *ApJ*, 870, 32
- Küpper, A. H. W., Maschberger, T., Kroupa, P., & Baumgardt, H. 2011, *MNRAS*, 417, 2300
- Kustaanheimo, P. & Stiefel, E. 1965, *Reine Angew. Math.*, 218, 204
- Lada, C. J. & Lada, E. A. 2003, *ARA&A*, 41, 57
- Lada, C. J., Lombardi, M., & Alves, J. F. 2009, *ApJ*, 703, 52
- Lada, C. J., Lombardi, M., & Alves, J. F. 2010, *ApJ*, 724, 687
- Lada, C. J., Margulis, M., & Dearborn, D. 1984, *ApJ*, 285, 141
- Lada, E. A., Depoy, D. L., Evans, Neal J., I., & Gatley, I. 1991, *ApJ*, 371, 171
- Lamers, H. J. G. L. M. & Gieles, M. 2006, *A&A*, 455, L17
- Lamers, H. J. G. L. M., Gieles, M., Bastian, N., et al. 2005, *A&A*, 441, 117
- Larsen, S. S. 2002, *AJ*, 124, 1393
- Larson, R. B. 1981, *MNRAS*, 194, 809
- Leinert, C., Zinnecker, H., Weitzel, N., et al. 1993, *A&A*, 278, 129
- Lombardi, M., Alves, J., & Lada, C. J. 2015, *A&A*, 576, L1
- Lüghausen, F., Parmentier, G., Pflamm-Altenburg, J., & Kroupa, P. 2012, *MNRAS*, 423, 1985
- Makino, J. 1991, *ApJ*, 369, 200
- Makino, J. & Aarseth, S. J. 1992, *PASJ*, 44, 141
- Marks, M. & Kroupa, P. 2011, *MNRAS*, 417, 1702
- Marks, M. & Kroupa, P. 2012, *A&A*, 543, A8
- Mason, B. D., Gies, D. R., Hartkopf, W. I., et al. 1998, *AJ*, 115, 821
- Megeath, S. T., Gutermuth, R., Muzerolle, J., et al. 2016, *AJ*, 151, 5
- Mikkola, S. & Aarseth, S. J. 1990, *Celestial Mechanics and Dynamical Astronomy*, 47, 375
- Oh, S. & Kroupa, P. 2016, *A&A*, 590, A107
- Oh, S., Kroupa, P., & Pflamm-Altenburg, J. 2015, *ApJ*, 805, 92
- Padoan, P., Nordlund, A., & Jones, B. J. T. 1997, *MNRAS*, 288, 145
- Pang, X., Li, Y., Tang, S.-Y., Pasquato, M., & Kouwenhoven, M. B. N. 2020, *ApJ*, 900, L4

- Perets, H. B. & Šubr, L. 2012, ApJ, 751, 133
- Pfalzner, S. 2019, arXiv e-prints [arXiv:1907.09712]
- Pflamm-Altenburg, J. & Kroupa, P. 2008, Nature, 455, 641
- Plunkett, A. L., Fernández-López, M., Arce, H. G., et al. 2018, A&A, 615, A9
- Porras, A., Christopher, M., Allen, L., et al. 2003, AJ, 126, 1916
- Portegies Zwart, S. F., McMillan, S. L. W., & Gieles, M. 2010, ARA&A, 48, 431
- Preibisch, T. & Zinnecker, H. 1999, AJ, 117, 2381
- Randriamanakoto, Z., Escala, A., Väisänen, P., et al. 2013, ApJ, 775, L38
- Reipurth, B. & Zinnecker, H. 1993, A&A, 278, 81
- Rogers, H. & Pittard, J. M. 2013, MNRAS, 431, 1337
- Röser, S. & Schilbach, E. 2019, A&A, 627, A4
- Röser, S., Schilbach, E., Piskunov, A. E., Kharchenko, N. V., & Scholz, R. D. 2011, A&A, 531, A92
- Sana, H., de Mink, S. E., de Koter, A., et al. 2012, Science, 337, 444
- Schmidt, M. 1959, ApJ, 129, 243
- Schneider, N., André, P., Könyves, V., et al. 2013, ApJ, 766, L17
- Selier, R., Heydari-Malayeri, M., & Gouliermis, D. A. 2011, A&A, 529, A40
- Spera, M. & Capuzzo-Dolcetta, R. 2017, Ap&SS, 362, 233
- Stephens, I. W., Gouliermis, D., Looney, L. W., et al. 2017, ApJ, 834, 94
- Stone, R. C. 1991, AJ, 102, 333
- Tanikawa, A., Hut, P., & Makino, J. 2012, New A, 17, 272
- Terlevich, E. 1987, MNRAS, 224, 193
- Tetzlaff, N., Neuhäuser, R., & Hohle, M. M. 2011, MNRAS, 410, 190
- Tout, C. A., Pols, O. R., Eggleton, P. P., & Han, Z. 1996, MNRAS, 281, 257
- Tutukov, A. V. 1978, A&A, 70, 57
- van den Bergh, S. & Lafontaine, A. 1984, AJ, 89, 1822
- Vazquez-Semadeni, E. 1994, ApJ, 423, 681
- Šubr, L., Kroupa, P., & Baumgardt, H. 2008, MNRAS, 385, 1673
- Wang, L., Iwasawa, M., Nitadori, K., & Makino, J. 2020, MNRAS, 497, 536
- Wang, L., Kroupa, P., & Jerabkova, T. 2019, MNRAS, 484, 1843
- Wang, L., Spurzem, R., Aarseth, S., et al. 2015, MNRAS, 450, 4070
- Weidner, C., Kroupa, P., & Bonnell, I. A. D. 2010, MNRAS, 401, 275
- Weidner, C., Kroupa, P., & Larsen, S. S. 2004, MNRAS, 350, 1503
- Weidner, C., Kroupa, P., & Pflamm-Altenburg, J. 2013, MNRAS, 434, 84
- Whitmore, B. C., Chandar, R., & Fall, S. M. 2007, AJ, 133, 1067
- Whitmore, B. C., Zhang, Q., Leitherer, C., et al. 1999, AJ, 118, 1551
- Winston, E., Hora, J. L., & Töls, V. 2020, AJ, 160, 68
- Yan, Z., Jerabkova, T., & Kroupa, P. 2017, A&A, 607, A126
- Zinnecker, H. & Yorke, H. W. 2007, ARA&A, 45, 481

## **Appendix A: Estimates of some observed quantities**

Figures 1 and 4 show the time dependence of the physical fraction of stars located within gravitationally bound clusters. However, many of these clusters contain only a small number of late type stars, and are not likely to be observed. The fraction of stars to be observed according to the criteria in Sect. 4.5 is plotted in Fig. A.1.

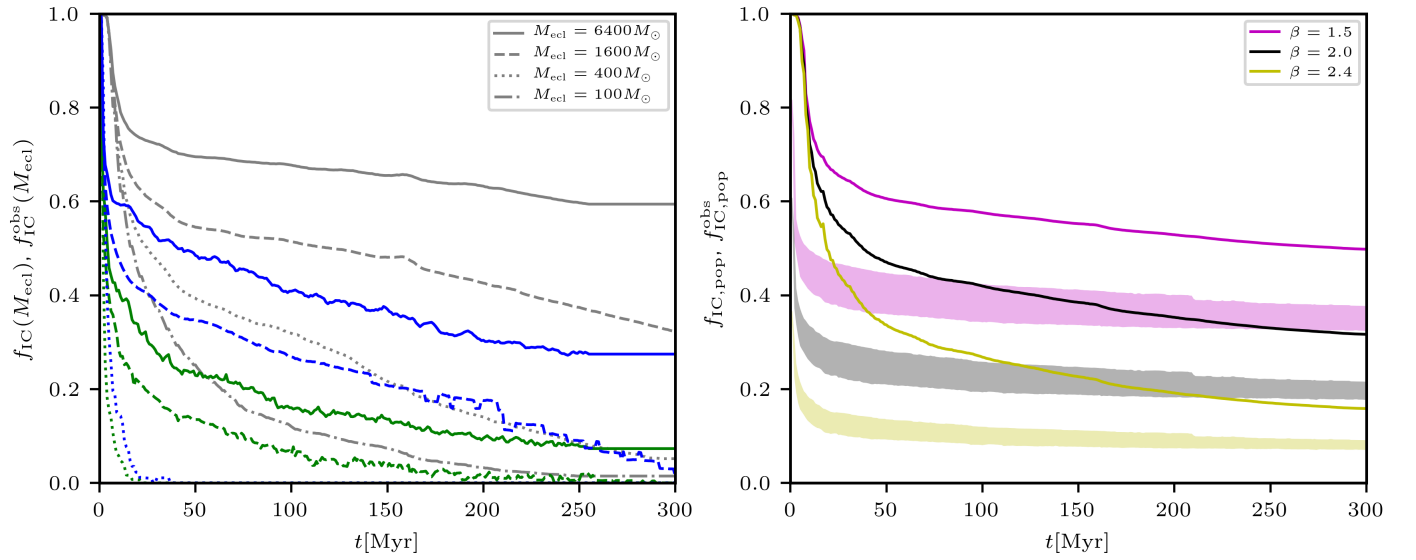


**Fig. A.1.** LEFT PANEL: The physical fraction of stars in clusters (gray lines; the same as Fig. 1), and the estimated observed fraction of stars in clusters when using  $r_{\text{search}} = 5$  pc (blue lines) and  $r_{\text{search}} = 2$  pc (green lines). The cluster mass is indicated by the line style. RIGHT PANEL: The physical fraction of stars in clusters (solid lines), and the estimated observed fraction of stars in clusters assuming  $r_{\text{search}}$  between 2 to 5 pc (filled areas). This panel is for the ECMF of eq. (4) with  $\beta = 1.5$  (magenta),  $\beta = 2$  (black), and  $\beta = 2.4$  (yellow).